Version of Record: https://www.sciencedirect.com/science/article/pii/S027737912100113X
Manuscript_adbcf11c62f646ca01533ac89ba7be03

Last millennium hydroclimate in the central equatorial North Pacific (5°N, 160°W)

Julian P. Sachs[1]*, Ines Mügler[1,^], Dirk Sachse[2], Matthew Prebble[3], Matthew Wolhowe[1]

[1]University of Washington, School of Oceanography, Box 355351, Seattle, WA 98195, USA

[2] GFZ German Research Centre for Geosciences, Section 4.6 Geomorphology, Organic Surface, 14473 Potsdam, Germany

[3] Australian National University, Department of Archaeology and Natural History, School of Culture, History and Languages, College of Asia and the Pacific, Canberra ACT 0200, Australia

* corresponding author (jsachs@uw.edu)

^Present Address: Dr. Ines von Borries, Universität Hamburg, Mittelweg 177; 20148 Hamburg
ines.muegler@uni-hamburg.de

Keywords: hydrogen isotopes, δ^2H, deuterium, lipid biomarkers, sterols, triterpenoids, peat sediment, lake sediment, Teraina, Washington Island, Northern Line Islands, tropical Pacific climate, tropical hydroclimate, late Holocene, last millennium, Little Ice Age, Medieval Warm Period, Medieval Climate Anomaly

Revision submitted to *Quaternary Science Reviews*

Abstract

Hydrogen isotope ratios ($^2H/^1H$ or δ^2H) were measured in lipid biomarkers from algal, plant and microbial sources in sediment cores from a lake and a peat bog on the small, sparsely-inhabited Washington Island (4°43'N, 160°25'W) to assess central equatorial Pacific hydroclimate conditions during the last millennium. High δ^2H values in lipids from a variety of biological sources indicate that the driest period of the last millennium occurred ~1450-1600 CE, during the first half of the Little Ice Age (LIA; 1450-1850 CE). An Intertropical Convergence Zone (ITCZ) located south of its modern position, less frequent and/or weaker El Niño events, and/or a La Niña-like mean state in the tropical Pacific were potential causes for this drying at Washington Island. From ~1600-1650 CE, an abrupt transition to modern-like low δ^2H values in phytoplankton, plant, and microbial lipids occurred, signaling the establishment of a high-rainfall regime similar to that observed today. This transition coincided with increased ENSO variability, an excess of central Pacific relative to eastern Pacific El Niños, and a decline in the zonal SST gradient across the tropical Pacific, reflecting an El Niño-like mean state. The Medieval Warm Period (MWP; 900-1250 CE) was characterized by high δ^2H values in lipids from phytoplankton (dinosterol, dinostanol), bacteria (hop-21-ene), and vascular plants (sitostanol), and by extension a drier climate relative to the modern lake. An increasing δ^2H trend through the MWP in lipids from all sources implies drying as Northern Hemisphere temperatures declined from the early to the late MWP. This drying is hypothesized to have been driven by extensive volcanism in northern, southern, and tropical latitudes, all of which tend to cause zonal mean drying at the latitude of WI (5°N). Finally, the transition period between the LIA and MWP ~1250-1450 CE was characterized by declining δ^2H values of plant and microbial lipids in peat sediments, indicating a trend toward wetter conditions; in the absence of known internal or external climate forcings, this may have been a regional or local event. This study demonstrates that the application of compound-specific δ^2H measurements of lipids from multiple biological sources and in multiple sedimentary archives from a single location can yield hydroclimate reconstructions with higher confidence than those based on single lipids. Such reconstructions are particularly important in the vast tropical Pacific, where few hydroclimate records exist.

1. Introduction

Reconstructions of climate from preindustrial times provide a benchmark against which modern climate variations can be assessed. The tropics, particularly the tropical Pacific owing to its sheer size, play an outsized role in the climate system since it is there that solar radiation receipts exceed losses to space. In addition, tropical Pacific climate perturbations, such as the El Niño-Southern Oscillation (ENSO), are projected throughout the globe. Yet, outside the monsoon-dominated western tropical Pacific, few multi-century paleoclimate records exist from the tropical Pacific Ocean against which we may make assessments of modern climate variation. This stems from the scarcity of islands in the central equatorial Pacific (few lacustrine or terrestrial records), the weak impact of hydroclimate on ocean chemistry (ambiguous marine biomineral records), and the low amplitude of temperature changes on seasonal-to-orbital timescales. Furthermore, the accumulation rate of sediment on the seafloor is slow, averaging about 1-2 cm kyr^{-1}, leaving sedimentary paleoclimate signals highly susceptible to smoothing via bioturbation.

Two prominent climate epochs characterized the preindustrial Common Era: the Medieval Warm Period (MWP, also known as the Medieval Climate Anomaly: ~900-1250 CE) and the Little Ice Age (LIA: ~1450-1850 CE) (Crowley, 2000; Lamb, 1965; Mann et al., 2009). Of the two, the LIA is more prominent in global climate reconstructions (Ahmed et al., 2013), with global cooling linked primarily to increased volcanism and reduced solar irradiance, with smaller contributions from lower atmospheric CO_2 and land-use changes (Atwood et al., 2016). The mean state of the monsoon-dominated western tropical Pacific during the last millennium has been extensively reconstructed from cave deposits, corals, and marine and lacustrine sediments (see compilations by (Denniston et al., 2016; Yan et al., 2015) and references therein). Together these records imply weakening of both the Asian and Australian monsoons during the LIA compared to the MWP, and either a contraction of the Intertropical Convergence Zone (ITCZ) or a southward shift of its northern boundary (Denniston et al., 2016; Yan et al., 2015). Uncertainty remains, however, for the record-sparse central and eastern tropical Pacific.

One of the primary methods for reconstructing hydroclimate from Pacific islands is the hydrogen isotope composition of lipid biomarkers ($^2H/^1H$ or δ^2H). The δ^2H values of lipids produced by plants, phytoplankton and cyanobacteria have been shown to be highly correlated

with the δ^2H values of environmental water, a proxy for hydroclimate conditions (Englebrecht and Sachs, 2005; Huang et al., 2004; Sachse et al., 2012; Sauer et al., 2001; Smittenberg et al., 2011; Zhang and Sachs, 2007). The ca. 100-400‰ ^2H-depletion of lipids relative to environmental water is the result of isotopic fractionation during lipid biosynthesis (Sachse et al., 2012; Sessions et al., 1999; Zhang and Sachs, 2007). The magnitude of this depletion in microalgae can be influenced by salinity (Chivall et al., 2014; Heinzelmann et al., 2015; Maloney et al., 2016; Sachs et al., 2016; Schouten et al., 2006; Weiss et al., 2017), irradiance (Sachs et al., 2017; van der Meer et al., 2015), growth rate (Sachs and Kawka, 2015; Zhang et al., 2009), and growth phase (Wolhowe et al., 2009; Wolhowe et al., 2015), whereas in terrestrial plants, transpiration causes isotopic enrichment of leaf water prior to lipid biosynthesis (Kahmen et al., 2013; Sachse et al., 2012). Salinity is the most extensively-studied environmental control on $^2H/^1H$ fractionation in microalgae. Both laboratory experiments (Chivall et al., 2014; Heinzelmann et al., 2015; Maloney et al., 2016; Sachs et al., 2016; Schouten et al., 2006; Weiss et al., 2017) and field studies (Nelson and Sachs, 2014a; Nelson and Sachs, 2014b; Sachs and Schwab, 2011; Sachse and Sachs, 2008) demonstrate that $^2H/^1H$ fractionation between water and lipids decreases (δ^2H_{lipid} increases) by ~1-2‰ ppt^{-1} when salinity increases across a wide range of lipids and environmental settings. $^2H/^1H$ fractionation is commonly expressed by the fractionation factor α_{lipid} ($\alpha_{lipid} = (1000 + \delta^2H_{lipid}) / (1000 + \delta^2H_{water})$), resulting in a salinity response of 0.001-0.002. As such, aquatic lipid biomarker δ^2H values from sedimentary archives have been used to reconstruct changes in salinity when additional constraints on source water δ^2H values were available (Nelson and Sachs, 2016; Sachs et al., 2018a; Sachs et al., 2009; Sachs et al., 2018c; Smittenberg et al., 2011; van der Meer et al., 2007; Vasiliev et al., 2017; Vasiliev et al., 2013; Vasiliev et al., 2019).

Sachs et al. (2009) applied δ^2H values of lipid biomarkers from lake sediments in Palau (7°N, 134°E) and the Galápagos (1°S, 89°W), and of bulk lipid extracts from lake sediments on Washington Island (a.k.a. Teraina; 5°N, 160°W), to show that the northern part of the ITCZ (Palau and Washington Island) became drier during the LIA, while the southern part (Galápagos) became wetter, from which they inferred a southward shift of the Pacific ITCZ. This finding was reinforced by subsequent studies suggesting a dry Palau (Richey and Sachs, 2016; Smittenberg et al., 2011) and a wet Galápagos (Atwood and Sachs, 2014; Nelson and Sachs, 2016) during the

LIA that were based on δ^2H values of source-specific lipid biomarkers. Yet the dry conditions at Washington Island during the LIA inferred from elevated bulk-lipid δ^2H values by Sachs et al. (2009) have not been verified with δ^2H values of source-specific lipids or any other hydroclimate proxy beyond the presence of halotolerant microbes in the microbial mat sediment. Those bulk δ^2H values incorporate changes in the net isotope fractionation in vascular plants (both terrestrial and aquatic), algae, and microbes that likely respond to hydroclimate changes differently. For example, terrestrial plants can respond to hydroclimate changes by varying their evapotranspiration rates, with resultant effects on plant lipid δ^2H values, a response not available to algae or bacteria (Sachse et al., 2012). Phytoplankton and cyanobacteria lipid δ^2H values respond to changes in salinity of the water in which they grow (Maloney et al., 2016; Sachs et al., 2016; Sachse and Sachs, 2008), a response not documented in terrestrial plants other than mangroves that display a lipid δ^2H response to salinity opposite that of phytoplankton (Ladd and Sachs, 2015a, b). Also complicating the bulk lipid δ^2H signal in a lake (particularly one that underwent a change from saline to fresh) is the fact that the relative abundance of lipids from these different sources over time may well have changed as the hydroclimate changed, weighting the bulk δ^2H value of sedimentary lipids more toward one source or another. This could be particularly significant if the relative abundance of acetogenic and isoprenoid lipids changed over time, as within a single plant, alga, or microbe the δ^2H value of lipids from these two biosynthetic pathways typically differ by 100‰ or more (Chikaraishi and Naraoka, 2005; Chikaraishi et al., 2004; Maloney et al., 2016; Sachs and Kawka, 2015; Sachs et al., 2017; Sachs et al., 2016; Sauer et al., 2001; Sessions et al., 1999; Zhang and Sachs, 2007). Given the importance of the central equatorial Pacific to any inferences about past ITCZ movements, confirmation of the bulk lipid δ^2H signal representing an aridification at Washington Island during the LIA is needed.

Here we apply δ^2H_{lipid} from plants, microalgae, and bacteria in two distinct sedimentary archives, a lake and a peat bog, to reconstruct hydroclimate variations on Washington Island, central tropical North Pacific, during the last millennium. By measuring δ^2H values in a diverse set of triterpenoid lipids from a variety of source organisms, and doing this in both a lake sediment core and a peat bog core, we develop a record of rainfall changes from Washington Island spanning the last millennium. Once developed, we compare rainfall changes at

120 Washington Island to published records of hydroclimate variability in the tropics and climate
121 forcing records in order to improve understanding of last millennium climate variations in the
122 tropical Pacific.
123
124 **2. Materials and Methods**
125 *2.1 Study site*
126 The small lens-shaped atoll of Washington Island, locally known as Teraina (14.2 km^2),
127 is located at 4°43'N, 160°25'W in the Central tropical Pacific (**Fig. 1**). It is under the influence
128 of the ITCZ much of the year and receives 2903 mm of rain annually ((Saenger et al., 2006) and
129 references therein). A freshwater lake (hereafter referred to as Washington Lake) of 2.4 km^2 that
130 occupies much of the eastern half of the island today was formerly a lagoon, based on the
131 presence of relatively pristine submerged coral heads and reef structures. Two vegetated
132 wetlands occur west of the lake, here referred to as eastern (0.6 km^2) and western (0.5 km^2) bogs
133 (**Fig. 1C**). They are dominated by *Scirpus littoralis* that has formed a sedge peat (Wester et al.,
134 1992). Marine mollusk shells and coral sands beneath the peat bogs imply they were formerly
135 part of the lagoonal basin occupied by the lake. The lake level is about 1 m above sea level
136 (Wester et al. 1992). A reef structure defines the western shore of the lake, and the construction
137 of a canal around 1900 CE may have caused water to flow from the lake into the eastern peat
138 bog, causing its degradation, though it is unclear whether the lake and bog were isolated prior to
139 this (Wester et al., 1992). The process and timing of the transition from marine-lagoon to
140 freshwater-lake are uncertain, but the earliest historical documentation of the freshwater dates to
141 1798 CE when the explorer Edmund Fanning described the environmental setting of the island as
142 similar to today (Sachs et al., 2009; Wester et al., 1992).
143 The physical and chemical characteristics of Washington Lake are described in Saenger
144 et al. (2006) and Sachs et al. (2009). In brief, the lake is well mixed, has a maximum depth of 3.7
145 m, and drains to the ocean through two low points in the coral rim (Saenger et al., 2006). Inflow
146 of marine water to the lake is not reported, and our measurements of slightly lower salinities in
147 the canal through which the lake drains to the sea, relative to the lake itself (0.2 vs. 0.9 PSU),
148 support this supposition. The hydrogen isotope composition of the lake water averaged -6.7‰ in
149 July 2005 (**Table 1**), similar to the predicted mean annual δ^2H value of precipitation of -6 ± 5‰

150 at the location of Washington Island from the Global Network of Isotopes in Precipitation
151 database (GNIP), as calculated by the Online Isotopes in Precipitation Calculator version 3.1
152 (OIPCv3.1) (Bowen, 2017; Bowen and Revenaugh, 2003; IAEA/WMO, 2015). The δ^2H value of
153 four rain samples collected July 6-8, 2005 averaged -22.1 ± 10.4‰ (**Table 1**).
154
155 *2.2 Field Sampling*
156 During July 2005 sediment cores from the freshwater lake and peat bogs were recovered
157 that reached the underlying coral basement at both locations (**Fig. 1C**). A detailed description of
158 the sampling, treatment, and depositional units of the Washington lake sediment cores is given in
159 Sachs et al. (2009). In short, sediment core WL2 (7.3 m long) was collected from the deepest
160 basin of Washington Lake at 4°41.0'N, 160°22.5'W at a water depth of 3.7 m, in sequential 1-m
161 sections using a 5 cm-diameter Colinvaux-Vohnout Livingstone-type rod-operated piston corer
162 (Geocore, Columbus, Ohio). Core sections were stored at 4°C or -20°C until they were sub-
163 sampled in 1 cm intervals. A basal ^{14}C age of 2965 yr BP was obtained on bulk organic matter,
164 and four depositional units were identified by Sachs et al. (2009). Authigenic calcium carbonate
165 at the bottom of the core (unit IV, 571-730 cm) is inferred to have been deposited in an open
166 lagoon. Two sequences of red-orange microbial mat differing in their texture and dominant
167 cyanobacterial species (unit III, 230-571 cm and unit II 112-230 cm) are inferred to have formed
168 under hypersaline conditions. Unconsolidated organic rich mud (gyttja), inferred to have been
169 deposited in the freshwater lake observed today comprises the uppermost unit (unit I, 0-112 cm).
170 A 50 cm peat core (WL-BG-PTC1) was recovered at 4°41.2'N, 160°23.1'W with a
171 Russian peat (**Fig. 2A**) borer in the eastern bog, approximately 25 m north of the canal (**Fig. 1C**).
172 Sediment depths in the vicinity of core WL-BG-PTC1 were observed to be uniformly ~50 cm,
173 bottoming on hard carbonate material or impenetrable sand. The peatland was dry and firm with
174 interspersed soft patches that were inundated and unable to support a person's weight (**Fig. 2B**).
175 The peat core was sub-sampled in 1 cm slices in the field and stored at 4°C.
176 Suspended particles were collected from the lake near the sampling site of WL2 via
177 filtration onto pre-combusted glass fiber filters (Whatman GF/F, 293 mm diam., 0.7 µm pore
178 size). Water for hydrogen isotope analysis was collected from the lake, the open ocean, and from

precipitation during four rain events. Surface salinity and water temperature data from multiple locations and times in the lake, canal, peat bog, and ocean are described in Saenger et al. (2006).

Leaves from the primary vegetation types in and around the peat bog and around the lake were sampled in order to determine the source of lipids in the lake and peat sediments. Images of these plants are shown in **Fig. S1**.

2.3 Lipid extraction and purification

Sediment, peat and vegetation samples were freeze dried before 0.5-1g of material was extracted with an Accelerated Solvent Extractor (ASE 200, Dionex Corp., Sunnyvale, CA, USA). Each sample was extracted twice with dichloromethane and methanol (DCM:MeOH, 9:1) at 100°C and 1500 psi for 5 min in 3 cycles. Total lipid extracts (TLE) were subsequently dried under a stream of N_2 with a Turbovap solvent evaporator (Caliper, Hopkinton, MA, USA).

Prior to accelerated solvent extraction, freshly defrosted particulate samples on GF/F filters were sonicated in acetone for 10 min and the solvent removed under a stream of nitrogen. The wet extracted material was then recombined with the total lipid extract after ASE extraction.

TLEs from the lake sediments, peat deposits, and GF/F filters were separated into neutral and polar fractions on aminopropyl impregnated silica gel in cartridge style SPE columns with dichloromethane:isopropyl alcohol (DCM:IPA, 3:1) and 4% acetic acid in diethyl ether, respectively. Neutral fractions were further separated using column chromatography with silica gel (5% water deactivated) into hydrocarbons (100% hexane), ketones (hexane:DCM, 1:1), sterols/alcohols (ethyl acetate:hexane, 1:4) and polar lipids (100% methanol). Only the hydrocarbon and sterol/alcohol fractions are discussed within the scope of this paper.

Aliquots of the sterol/alcohol fractions of sediment extracts and TLEs from vegetation samples were dried and re-dissolved with 20 µL pyridine and 20 µL bis (trimethylsilyl) trifluoroacetamide (BSTFA, Sigma Aldrich, St. Louis, MO, USA). The mixture was heated (60°C; 30 min) to convert alcohols into their corresponding trimethylsilyl ethers. After addition of an internal standard (5α-cholestane, Sigma Aldrich, St. Louis, MO, USA) in toluene, the derivatized sterol/alcohol fractions and the hydrocarbon fractions were analyzed by gas-chromatography-mass spectrometry (GC-MS) to identify the lipids present and determine their purity. The 6890N GC (Agilent, Santa Clara, CA, USA) was equipped with an Agilent 5983

autosampler, a split-splitless injector operated in splitless mode, a HP-5ms column (30 m x 0.32 mm i.d. x 0.25µm film thickness, Agilent) and interfaced to an Agilent 5975 quadrupole mass selective detector (MSD). The detector was operated at 70eV with a mass range of m/z 50-700 at 2.28 scans s^{-1}. Target compounds were identified based on GC-retention times, by comparison with mass spectra of standard compounds (stigmasterol, β-sitosterol, sitostanol) and with published mass spectra. Quantification of target lipids was performed with a gas chromatograph-flame ionizaion detector (GC-FID). The Agilent 6890 GC was equipped with an Agilent 5983 autosampler and a PTV injector operated in splitless mode. A DB5-MS column (60 m x 0.32 mm x 0.25 µm) was used with He as carrier gas (2.5ml min^{-1}). The oven temperature was increased from 60°C to 220°C at 40°C min^{-1}, then at 2°C min^{-1} to 325°C where it was held for 7 min. Quantification was performed by comparing integrated peak areas with that of the 5α-cholestane internal standard.

2.4 Triterpenoid purification by HPLC-MS

To further purify lipids of interest for subsequent hydrogen isotope analysis, selected sterol/alcohol fractions were further processed by reverse-phase high-performance liquid chromatography-mass spectrometry (RP-HPLC-MS; Agilent 1100, Santa Clara, CA, USA) using a procedure modified from Smittenberg and Sachs (2007) and Atwood and Sachs (2012). In brief, an Agilent Zorbax C_{18} column (250 mm x 4.6 mm) maintained at 30°C was used for chromatographic separation. The sterol/alcohol fractions were dissolved in 25 µL DCM:MeOH (2:1). 5% water in MeOH was delivered to the column isocratically for 65 min at 1.5 mL min^{-1}, followed by 100% ethyl acetate for 10 min at 2.0 mL min^{-1} to clean the column. A makeup flow of MeOH was delivered at 0.3 mL min^{-1} to the 5% of the solvent stream that was split off to the MS. Elution of target lipids was monitored by extracting ions at *m/z* 411 (dinosterol), *m/z* 397 (β-sitosterol), *m/z* 399 (sitostanol), and *m/z* 395 (stigmasterol), and by obtaining mass spectra in full scan mode (*m/z* 200-800). Depending on the sample concentration, retention times of target compounds typically varied by ~ ± 30 s. 1-min-long fractions were collected and recombined when containing ~2% or more of the target compound as determined by HPLC-MS and/or GC-MS in order to ensure quantitative recovery and avoid $^{2}H/^{1}H$ fractionation that occurs across HPLC peaks (Atwood and Sachs, 2012; Smittenberg and Sachs, 2007). All (recombined)

samples were analyzed by GC-FID and GC-MS before and after HPLC purification to quantify analytes, assess recoveries, and confirm peak purities.

2.5 Hydrogen isotope analysis of lipids

HPLC-purified triterpenoids were dissolved in 20 µL pyridine and acetylated with 20 µL acetic anhydride of known isotopic composition (Dr. Arndt Schimmelmann, Indiana University) at 70°C for 30 min. Acetylated sterol fractions were dried under a stream of N_2 and re-dissolved in toluene containing the internal standard 5α-cholestane. Acetylated target compounds were quantified by comparing their integrated peak areas on GC-FID to that of the 5α-cholestane standard using GC conditions described above, then redissolved in toluene to a concentration of 200-300 ng μL^{-1} to ensure optimal signal intensity on the GC-irMS with a 1 µL injection. δ^2H values were not obtained when < ~0.3 µg of an analyte remained following the HPLC purification protocol.

Lipid δ^2H values were determined by GC-irMS on a Thermo DELTA V PLUS (Thermo Scientific, Waltham, MA, USA). The gas chromatograph (Trace Ultra, Thermo) was equipped with a split-splitless injector operated in splitless mode at 280°C, a TRIPLUS autosampler (Thermo Scientific, Waltham, MA, USA) and a DB5-MS capillary column (60 m x 0.32 mm x 0.25 µm, Agilent). The oven temperature was increased from 80°C to 200°C at 20°C min^{-1}, then at 4°C min^{-1} to 320°C where it was held for 30 min. The helium flow was held constant at 1 mL min^{-1}. Compounds were pyrolized quantitatively to H_2 in a high-temperature conversion oven at 1420°C (Burgoyne and Hayes, 1998). 1 µL of purified, acetylated lipids was co-injected with 1 µL of an internal standard containing nC_{32} and nC_{38} alkanes of known hydrogen isotopic compositions (Dr. Arndt Schimmelmann, Indiana University). Co-injection standards were chosen to bracket target analytes in the GC chromatogram and the peak heights adjusted to match the target lipid. Isotope values were corrected using the two co-injection standards and expressed in the delta notation with Isodat 2.0 software (Thermo-Fischer, Bremen, Germany) according to the procedure described in Nelson and Sachs (2013). Sterol/alcohol δ^2H values were corrected for the hydrogen atoms in the added acetyl group by mass balance calculation (Nelson and Sachs, 2013). After every two samples (6 injections) a lab standard containing a mixture of n-alkanes (nC_{14} to nC_{36}) with known isotopic compositions (as determined by TC/EA-irMS) was

run to correct sample δ^2H values for instrument drift and to the VSMOW scale, as described in Nelson & Sachs (2013). Hydrogen isotopic values were determined in triplicate whenever sufficient material was available. The H_3^+ factor (Sessions et al., 2001) was determined daily using the reference gas and remained stable below 4 ppm nA^{-1} during the measurement period.

2.6. Sediment core chronologies

The chronology for Washington Lake sediment core WL2 is described in detail in Sachs et al. (2009). There, two age-depth models were constructed for the sedimentological units II and III. Here, because it agrees with the interpretation of the results associated with the peat core chronology, and in order to facilitate clarity, we only refer to age model b that applied a mixed atmospheric-marine calibration curve with a 15 ± 5 % contribution of marine bicarbonate. It should be noted, however, that we cannot rule out the correctness of the alternative age model which does not account for any potential reservoir effect. As described in Sachs et al. (2009) the upper 111 cm of core WL2 consists of unconsolidated brown organic-rich freshwater gyttja inferred to be bioturbated based on bomb ^{14}C present in bulk organic carbon from 33, 83, 101, and 111 cm (Sachs et al., 2009). We thus make the conservative assumption that the upper 111 cm of sediment was deposited since 1950 CE (approximately the beginning of widespread above-ground nuclear testing). For the purposes of this study, we then assign an age of 2005 CE for the core top (year of collection) and an age of 1983 for the samples at 10 & 15 cm, the midpoint between 1950 and 2005 CE. This is useful for plotting the data but has little or no bearing on its interpretation.

The chronology for Washington Island peat core WL-BG-PTC1 was constructed from six ^{14}C dates, three each on humin and bulk organic material (**Table 2**). A Bayesian age model for the core was created using the Bacon software package in R (Blaauw and Christen, 2011) which calibrated the ^{14}C dates using IntCal13 (Reimer et al., 2013) (**Fig. 2C** & **Table 2**). A model age of 1468 CE for the 0-1 cm interval of sediment implies that sediment accumulation either ceased in the mid-15th century or that more recent sediments have been denuded. Wester et al. (1992) concluded, in fact, that the eastern bog (which we cored) showed evidence of disturbance or degradation (Wester et al., 1992). The sediment character changed from fibrous macroscopic plant debris at the bottom to finer gyttja-like sediment at ~23 cm (**Fig. 2A)**, suggesting an abrupt

change in sedimentation conditions potentially related to the water depth at the core site. This macroscopic observation agrees well with palynological evidence that suggests a transition from sedges to ferns as the dominant vegetation at this core depth (**Table S1**).

3 Results

3.1 Lipid sources and concentrations

The biological origin of triterpenoid lipids in lake and peat sediments was determined by comparing mass spectra of analytes of interest with mass spectra of lipids extracted from (1) terrestrial vegetation voucher samples collected on Washington Island in July 2005 (**Fig. S1**), (2) suspended particulate samples filtered from Washington Lake in July 2005, and (3) published reference mass spectra. From this analysis lipids were assigned to classes representing vascular plants, bacteria, or microalgae (**Table 3**).

3.1.1 Triterpenoids from plants and ferns

All plant specimens, suspended particles from Washington Lake, and surface sediments from both the peat bog and lake contained the C_{29} sterols β-sitosterol (24β-ethyl-cholest-5-en-3β-ol, $C_{29}H_{50}O$) and stigmasterol (stigmasta-5,22-dien-3β-ol or 5,22-cholestadien-24-ethyl-3β-ol, $C_{29}H_{48}O$) (**Table 3**). Both are among the most common sterols in plants (Gaskell and Eglinton, 1976; Goad and Goodwin, 1972; Grunwald, 1975; Huang and Meinschein, 1979; Volkman, 1986; Wen-Yen and Meinschein, 1976) and are also produced by several phytoplankton groups (Volkman, 2003; Volkman, 1986). The C_{29} stanol sitostanol (24-ethyl-5α-cholestane-3β-ol, $C_{29}H_{52}O$; aka stigmastanol) was not detected in any of the plant samples, but occurred in the lake suspended particles and in surface sediments from both the lake and peat bog. It is produced in limited quantities by some plants and microalgae (Nishimura and Koyama, 1976) but its primary source is thought to be microbial reduction of β-sitosterol during early diagenesis (Wakeham, 1989), a process widely believed to produce most stanols in lacustrine and marine sediments (Gaskell and Eglinton, 1975, 1976; Nishimura, 1978; Nishimura and Koyama, 1976). Together β-sitosterol, stigmasterol, and sitostanol in Washington Island lake and

bog sediments are considered to be indicators of vascular plant input with smaller contributions from microalgae.

The C_{30} triterpene fern-7-ene occurred in all four fern specimens sampled in and around the bog and lake, and in surface sediments from both locales, but was not detected in lake suspended particles or any of the other plant samples (**Table 3**). This and related fernenes are common trterpenoid lipids in many fern species (Ageta and Arai, 1983; Ageta et al., 1963; Bottari et al., 1972), but can also have a microbial source in some environments (Howard et al., 1984; Schouten et al., 2001; Volkman et al., 1986). Given the widespread occurrence of ferns in and around the bog and lake on Washington Island and the presence of fern-7-ene in all fern specimens sampled, we consider this lipid to be primarily an indicator of vascular plant input to lake and bog sediments with microbes a potential secondary source.

3.1.2 Triterpenoids from phytoplankton

Dinosterol (4α-23,24-trimethyl-5α-cholest-22E-en-3β-ol, $C_{30}H_{52}O$) and dinostanol (4α,23,24-trimethyl-5α-cholestan-3β-ol, $C_{30}H_{54}O$) occurred in suspended particles from the lake and surface sediments from both the lake and bog, but not in any of the plant samples (**Table 3**). These two 4-methyl sterols are produced almost exclusively by dinoflagellates in freshwater and marine systems and are widely used as biomarkers for dinoflagellates (Atwood et al., 2014; Boon et al., 1979; Leblond and Chapman, 2002; Piretti et al., 1997; Robinson et al., 1984; Volkman, 2003; Volkman et al., 1998), though they can be produced in minor amounts by a small number of other taxa (Volkman et al., 1993). Together they are assumed in this study to derive from microalgae.

3.1.3 Triterpenoids from bacteria

Diploptene (hop-22(29)-ene) occurred in all four fern specimens as well as in surface sediments from the lake and bog, but not in the other plants or in lake suspended particles (**Table 3**). Hope-21-ene occurred in only one plant sample, the fern *Microsporum scolopendrium*, as well as in surface sediments from the lake and bog, but not in lake suspended particles (**Table 3**). A C_{27} hopane occurred in surface sediments from the bog but not in surface sediments or suspended particles from the lake, nor in any plant samples (**Table 3**). Hopanoids such as these are pentacyclic triterpenoids produced almost exclusively by bacteria (Belin et al., 2018;

Kannenberg and Poralla, 1999; Ourisson et al., 1979; Ourisson et al., 1987; Volkman, 2005) and are important membrane components in both Gram-negative and Gram-positive bacteria (Hefter et al., 1993; Kannenberg and Poralla, 1999; Ourisson et al., 1979; Rohmer et al., 1992; Rohmer et al., 1984).

Diploptene is synthesized by all hopanoid-containing bacteria (Ourisson et al., 1987), including cyanobacteria, purple non-sulfur bacteria, methanotrophic bacteria, and anammox bacteria (Douka et al., 2001; Härtner et al., 2005; Rohmer et al., 1984; Simonin et al., 1996; Sinninghe Damsté et al., 2004). It is ubiquitous in the geosphere, being found in soils, microbial mats, peat deposits, marine and lacustrine sediments, and frequently used as a molecular marker for bacteria (Elvert et al., 2001; Hanisch et al., 2003; Kaiser et al., 2016; Prahl et al., 1992; Ries-Kautt and Albrecht, 1989; Sinninghe Damsté et al., 2004; Xu and Jaffé, 2008). Diploptene is also produced by some higher plants, particularly ferns (Ageta and Arai, 1983; Anderson et al., 1979; Inayama et al., 1989) - consistent with its occurrence in all four fern specimens we sampled (**Table 3**), as well as certain mosses (Huang et al., 2010; Toyota et al., 1998).

Hop-21-ene is produced by both aerobic and anaerobic bacteria (Douka et al., 2001; Härtner et al., 2005; van Winden et al., 2010; Welander et al., 2010) as well as some species of ferns (Shiojima and Ageta, 1990). It can also be produced diagenetically from diploptene (Sinninghe Damsté et al., 2014). C_{27} hopanes in recent peat sediments and soils (Ries-Kautt and Albrecht, 1989) as well as ancient sediments (Freeman et al., 1990) have been linked to bacteria. This is consistent with its presence in sediments from the peat bog but not in any of the plant samples or the suspended particles in the lake. Because hopanoids are ubiquitous in bacteria and produced only sparingly by plants or algae (such as diploptene production by ferns) (Kannenberg and Poralla, 1999; Ourisson et al., 1987) we ascribe the presence of the three hopanoids diploptene, hop-21-ene, and C_{27} hopane in the lake and bog sediments primarily to production by bacteria with a secondary contribution from ferns.

3.1.4 Downcore lipid concentrations

Triterpenoid concentrations in Washington Lake sediments were between 2-154 µg g^{-1} for the phytoplankton lipids dinosterol (5-154 µg g^{-1}) and dinostanol (2-122 µg g^{-1}), which generally covaried, 0.5-108 µg g^{-1} for the vascular plant lipids sitostanol (2-62 µg g^{-1}) and

fernene (0.5-108 μg g^{-1}), and 0.2-171 μg g^{-1} for the bacterial lipid hop-21-ene (**Table 4, Fig. S2A**). Concentrations of the two phytoplankton lipids were highest in the lower section of the core (580-350 cm) (**Fig. S2A**) covering the period 900-1286 CE (**Fig. 3A**), exceeding those from vascular plants (sitostanol and fernene) and bacteria (hop-21-ene). From 1328-1643 CE there were no consistent relationships between lipids from the three sources (**Fig. 3A**).

In the peat sediments the concentrations of vascular plant lipids β-sitosterol (1.2-37 μg g^{-1}) and sitostanol (1.2-85 μg g^{-1}) exceeded the concentrations of dinostanol (3.5-13 μg g^{-1}) from phytoplankton in all but the shallowest two samples (**Table 5, Fig. S2B**) deposited from 1620-1640 CE (**Fig. 3B**). They also exceeded the concentrations of diploptene (0.4-2.6 μg g^{-1}) and the C_{27} hopane (0.4-1.7 μg g^{-1}), both from bacteria, at all depths except at 10 cm where both plant lipids reached their lowest concentration, slightly less than that of the hopane which reached its highest value at that depth. The primary trend in triterpenoid concentrations was a decrease for all but the hopane between ~1150-1350 CE, followed by a smaller increase for the two plant sterols and little or no consistent change for the other lipids between ~1350-1420 CE (**Fig. 3B**). Concentrations of the hopane decreased with the other triterpenoids from 1155-1210 CE, then rose to maximum values of 1.6-1.7 μg g^{-1} until 1420 CE. Highest hopane concentrations in the upper 25 cm of the peat core coincided with a transition from fibrous peat with to finer gyttja-like sediment at ~23 cm (**Fig. 2A**).

3.2 Hydrogen isotope values

The hydrogen isotope composition of water (rain, lake, and ocean) and lipids from lake suspended particles and sediments from the peat bog and lake were measured in order to reconstruct hydroclimate of Washington Island during the last millennium.

3.2.1 δ^2H values of water

δ^2H values of three rainwater samples collected on Washington Island on July 6, 2005 were between -21‰ and -34‰ (**Table 1**). A single rainwater sample collected just offshore on July 8, 2005 had a δ^2H value of -6‰, similar to Washington Lake surface water collected on July 6, 2005 which had a δ^2H value of -7‰ (**Table 1**). The average rain δ^2H value was -22 ± 10‰, with a median value of -24‰.

Surface seawater collected near Washington Island (2°N, 158°W) on July 8, 2005 had a δ^2H value of 3‰, the same as surface seawater near Christmas Island (4°N, 159°W) collected on July 10, 2005 (**Table 1**).

3.2.2 δ^2H values of triterpenoid lipids from Washington Lake

Average δ^2H values of phytoplankton sterols were more ^2H-depleted than triterpenoid lipids from vascular plants and bacteria (**Fig. S3A** and **Fig. 4A**). In lake sediments δ^2H values of dinosterol averaged -238 ± 40‰ while those of dinostanol averaged -253 ± 50‰ (**Table 6**). This compared to average δ^2H values of -223 ± 23‰ for sitostanol and -157 ± 20‰ for fernene from vascular plants, and -172 ± 23‰ for hop-21-ene from bacteria.

The lowest δ^2H values of phytoplankton sterols occurred in lake sediments deposited since 1950 CE, with dinosterol averaging -285 ± 7‰ and dinostanol averaging -301 ± 2‰ (**Fig. 4A**). This compared to post-1950 plant lipid δ^2H values of -245 ± 6‰ for sitostanol, -249 ± 1‰ for b-sitosterol, and -196 ± 11‰ for stigmasterol (**Fig. 4A**).

Modern suspended particles in Washington Lake had phytoplankton sterol δ^2H values that were similar to post-1950 sediment averages in the case of dinosterol (-292 ± 3‰ vs -285 ± 7‰, respectively), but ^2H-depleted in the case of dinostanol (-322 ± 6‰ vs -301 ± 2‰, respectively) (**Table 7**, **Fig. 4A**).

A pattern of increasing δ^2H values of lipids from microalgal, plant, and bacterial sources as well as the sediment total lipid extract characterized the period ~900-1300 CE in Washington Lake, corresponding to the Medieval Warm Period (**Fig. 4A**). Maximum δ^2H values of dinosterol and dinostanol from phytoplankton, and sitostanol from vascular plants occurred around 1330 CE.

A different temporal evolution of δ^2H values of fernene (plants) and the TLE (all sources) was observed whereby both reversed their increasing trend ~1280 CE and decreased until 1370-1390 CE. An increasing δ^2H trend characterized both time series during the first half of the Little Ice Age (~1400-1600 CE), during which time fernene δ^2H values averaged -143 ± 11‰ and TLE δ^2H values averaged -130 ± 8‰ (**Fig. 4A**). During the same time interval hop-21-ene δ^2H values (bacteria) averaged -156 ± 8‰, intermediate between pre-1200 CE (-159 ± 25‰) and post-1640 CE (-197 ± 3‰) values.

449 The aforementioned trends in lipid δ^2H values in Washington Lake sediments over the
450 last 1.1. ka are most evident when each δ^2H time series is standardized to Z-scores by subtracting
451 the mean and dividing by the standard deviation of the data series (**Fig. 5A**). This procedure
452 highlights δ^2H deviations from the average δ^2H values of each lipid over the full record.
453
454 *3.2.3 δ^2H values of triterpenoid lipids from peat sediments*
455 As in the lake sediments, the phytoplankton lipid dinostanol from the peat sediments had
456 a lower average δ^2H value than those for the plant and bacterial lipids (**Fig. S3B** and **4B**).
457 Dinostanol δ^2H values in the peat sediments averaged -200 ± 47‰ compared to -170 ± 14‰ and
458 -161 ± 13‰ for the plant lipids b-sitosterol and sitostanol, and -130 ± 38‰ and -153 ± 21‰ for
459 the bacterial lipids diploptene and C_{27}-hopane (**Table 8**). Most of the ^2H-depletion in dinostanol
460 relative to plant and bacterial lipids is attributed to their 110‰ decline from ~1230-1440 CE
461 (**Fig. 4B**). Prior to that time, from ~1150-1230 CE, lipids from all three sources had relatively
462 constant δ^2H values. From ~1230-1440 CE, all lipid δ^2H values declined (except for diploptene
463 which began its decline ~1260 CE). This two-step pattern is most clearly seen when the δ^2H
464 values of all lipids are shown as Z-scores as above (**Fig. 5B**). Standardized δ^2H values of all
465 lipids in the lake and peat sediment cores are plotted in **Fig. 7A** and **7B**, respectively.
466
467 **4. Discussion**
468 The hydrogen isotope composition of all plant, microalgal, and bacterial lipids in lake
469 and bog sediments is expected to reflect changes in the δ^2H value of precipitation, which in the
470 tropics is dominated by the 'amount effect' (Dansgaard, 1964; Kurita et al., 2009; Lee and Fung,
471 2008; Risi et al., 2008; Rozanski et al., 1993). Hence, during wetter (drier) climates, the δ^2H
472 values of these lipids is expected to decrease (increase). δ^2H values of phytoplankton lipids will
473 additionally reflect the salinity of the lake water owing to diminished (greater) $^2H/^1H$
474 fractionation at higher (lower) salinities (Schouten et al., 2006), with the magnitude of this
475 salinity effect approximately 1-2‰ ppt^{-1} (Gould et al., 2019; M'boule et al., 2014; Maloney et
476 al., 2016; Nelson and Sachs, 2014b; Sachs et al., 2016; Sachs and Schwab, 2011; Sachse and
477 Sachs, 2008). This makes δ^2H values of phytoplankton lipids, such as dinosterol and dinostanol,
478 particularly sensitive to hydroclimate changes in a saline lake since changes in the rainfall

regime would be expected to cause changes in (i) the δ^2H value of precipitation (via the amount effect), (ii) the lake salinity (through dilution or evaporation), and (iii) the lake water δ^2H (through the precipitation-evaporation balance). These three parameters drive δ^2H values of phytoplankton in the same direction, making them more negative in a wetter climate and more positive in a drier climate (Nelson and Sachs, 2016; Richey and Sachs, 2016; Sachs et al., 2018b; Sachs et al., 2009; Smittenberg et al., 2011).

4.1 Differences in δ^2H values between lipid sources and environments

The differences between the diverse set of lipid δ^2H records developed here reinforce the importance of applying multiple proxies when constructing the paleoenvironment, as each may be reflective of multiple environmental and biological processes. For example, the algal (dinosterol and dinostanol) and partially-algal (sitostanol) lipids in the lake core exhibit ^2H-enrichments from 1290-1330 CE, implying drying, while δ^2H values of fernene (from ferns) and the TLE (from all sources) both decrease, implying wetting (**Figs. 4A & 5A**). Factors that could have caused an increase in phytoplankton lipid δ^2H values, while those from ferns and the total lipid assemblage decreased, include a decrease in phytoplankton (e.g., dinoflagellate) growth rates (Sachs and Kawka, 2015), decreasing light levels (e.g., from greater turbidity or a deeper habitat, etc.) (Sachs et al., 2017), and/or a change in the relative abundance of different dinosterol-producing dinoflagellates. A 60-75% decrease in the concentration of dinosterol and dinostanol from 1290-1330 CE (**Fig. 3A**) may imply that growth conditions became less optimal for dinoflagellates in Washington Lake, consistent with these possibilities. Increasing salinity would also cause an increase in phytoplankton lipid δ^2H values, but would be more difficult to reconcile with the coincident decrease in fernene and TLE δ^2H values if the latter were the result of wetter conditions. An alternate possibility is that it did become drier on Washington Island 1290-1330 CE, but that higher plants responded by reducing evapotranspiration rates, which can cause plant lipid δ^2H values to decrease (Feakins and Sessions, 2010). If the lipid assemblage in the lake sediments was dominated by lipids from higher plants, this process could account for decreased δ^2H values of both fernene and the TLE.

Another example of δ^2H_{lipid} values from different sources diverging from each other in the same core occurs in the period from ~1250-1300 CE, when δ^2H values of diploptene (from

both ferns and bacteria) in peat bog sediments reached maximum values, coincident with a decrease in the δ^2H values of phytoplankton (dinostanol, sitostanol) and plant (β-sitosterol, sitostanol) lipids (**Fig. 4B**). Given the ubiquity of diploptene in bacteria and its occurrence in all fern specimens we sampled (**Table 3**), a possible explanation is that the contribution of this lipid from ferns increased relative to the contribution from bacteria. A marked increase in fern pollen beginning at 1260 CE (20 cm in the core; **Fig. S3**) supports this possibility. Ferns would be expected to have lipid δ^2H values more enriched than bacteria, on average, as a result of plant-water ^2H-enrichment during evapotranspiration (Sachse et al., 2012). Uncertainties in sediment core chronologies are sufficiently large that direct comparison with this ~50-yr time interval in the lake core is not possible.

A later discrepancy between δ^2H values of different lipids occurred ~1400 CE, when the TLE and fernene in the lake sediments became ^2H-enriched (**Fig. 4A** & **5A**) while lipids from all sources in the peat bog sediments were undergoing a century-long δ^2H decline (**Fig. 4B** & **5B**). The shift toward higher TLE and fernene δ^2H values in the lake sediments coincides with a subtle change in sediment lithology and the character of the microbial mat sequence comprising this section of the core, with Unit III (230–571 cm) transitioning to Unit II (112–230cm) at 230 cm, or 1405 CE (Sachs et al., 2009). Unit II is a gelatinous, red–orange microbial mat with abundant rod-shaped cyanobacteria from the *Aphanothece* morphotype, known to produce prodigious quantities of exopolysaccharide gel; Unit III is a red–orange microbial mat with a leather-like texture, interbedded with well-preserved 0.5–1 mm layers composed predominantly of empty sheaths of the filamentous cyanobacterium *Leptolyngbya* sp. and remnants of globular colony-forming cyanobacteria of the *Entophysalis* morphotype (Sachs et al., 2009). Sediment total lipid extracts usually contain far more fatty acids than isoprenoid lipids, and the former, being biosynthesized in the acetogenic pathway, are typically ~100‰ enriched in ^2H relative to lipids produced via the isoprenoid biosynthetic pathway, even when produced by the same organism (Chikaraishi and Naraoka, 2005; Chikaraishi et al., 2004; Maloney et al., 2016; Sachs and Kawka, 2015; Sachs et al., 2017; Sachs et al., 2016; Sauer et al., 2001; Sessions et al., 1999; Zhang and Sachs, 2007). If the microbial community that produced the post-1400 CE sediments (Unit II) in Washington Lake produced a greater quantity of acetogenic lipids, such as fatty acids, than those comprising the pre-1400 CE sediments (Unit III), it could account for the

transition to higher TLE δ^2H values (**Fig. 4A** & **5A**) at a time when all lipids in the peat bog sediments were becoming more ^2H-depleted (**Fig. 5B**). Another plausible explanation for this positive shift in the TLE δ^2H values could be an increase in the ratio of terrestrial-to-aquatic lipids, as the former are relatively ^2H-enriched due to evapotranspiration (Sachse et al., 2012; Sachse et al., 2004). The accompanying increase in lake-sediment fernene δ^2H values (**Fig. 5A**) may have been caused by an increase in the proportion of that lipid derived from ferns relative to bacteria (Howard et al., 1984; Schouten et al., 2001; Volkman et al., 1986), as other plant (beta-sitosterol and sitostanol), algal (dinostanol), and microbial (diploptene, hopane) lipids from the peat bog sediments are consistent with wetter conditions by 1420 CE (**Fig. 4B** & **5B**).

While many of the above proposed explanations for different δ^2H trends in different lipids and/or cores are largely speculative, they make it clear that a reliable precipitation reconstruction from Washington Island must consider the data collectively. Compared as z-scores and overlain, we observe the following primary trends in Washington Island hydroclimate during four time intervals of the last millennium: a drying trend 950-1250 CE (the Medieval Warm Period, MWP), wetting from 1250-1450 CE (the MWP-LIA transition), a somewhat dry, stable period 1450-1600 CE (the early LIA), and a wetter, 'modern' climate established by >1650 CE (the late LIA-modern period) (**Fig. 7A, B**). These are discussed below in the context of tropical Pacific and global climate conditions.

4.2 Last millennium hydroclimate variations at Washington Island

In response to the seasonal migration of the ITCZ, Washington Island experiences its driest conditions of the year during boreal winter (Jan-Mar, 2.8-3.9 mm d^{-1}), when the ITCZ moves south of the island, as compared to boreal summer (May-July, 10.1-11.6 mm d^{-1}) when the ITCZ sits north of the island (**Fig. 6A-C**). On interannual timescales, Washington Island is driest during La Niña years (here defined as Southern Oscillation Index, or SOI, > 1) when annual mean rainfall averages -0.6 mm d^{-1} relative to the 1981-2010 mean, compared to +1.5 mm d^{-1} during El Niño years (here defined as SOI < -1; GPCP v2.3 precipitation and SOI data provided by the NOAA/ESRL Physical Sciences Laboratory, Boulder Colorado from their Web site at http://psl.noaa.gov/) (**Fig. 6D,E**).

569 *4.2.1 Hydroclimate during the Medieval Warm Period: 950-1250 CE*

570 Northern Hemisphere temperatures decreased 0.6°C from a preindustrial high ~950 CE to
571 a Medieval low ~1100 CE and remained within 0.2°C of that value until the end of the Medieval
572 Warm Period ~1250 CE according to the reconstruction by Mann et al. (2008) (**Fig. 7J**). A
573 compilation of global surface temperature reconstructions from data and models shows more
574 muted variations during this time, with little clear indication of a MWP signal (Pages-2k-
575 Consortium, 2019). Increasing δ^2H values of lipids from phytoplankton (dinosterol, dinostanol),
576 plant (fernene), and bacteria (hop-21-ene) in Lake Washington sediments from ~950 to ~1250
577 CE indicate that Washington Island became drier through the MWP (**Fig. 7A**). Mechanisms that
578 could cause a 300 yr (950-1250 CE) drying trend at WI include a southward shift of the ITCZ,
579 greater frequency or intensity of La Niña events, and increased volcanic activity.

580 It is unlikely that a change in ENSO was the primary cause of WI drying 950-1250 CE, as
581 multiple lines of evidence point toward an increase in the frequency and/or intensity of El Niño
582 events over that time (Atwood and Sachs, 2014; Conroy et al., 2010; Conroy et al., 2008; Moy et
583 al., 2002), which would be expected to cause a wetter climate at WI (**Fig. 6D**). This evidence
584 includes: an increase in the grain size of sediment in El Junco Lake, Galápagos (Conroy et al.,
585 2008), an increase in the concentration and decrease in the δ^2H value of botryococcene lipids in
586 El Junco Lake, Galápagos (Atwood and Sachs, 2014; Sachs et al., 2009; Zhang et al., 2014), and
587 an increase in the frequency of red sediment deposition in Laguna Pallcacocha, Ecuador (Moy et
588 al., 2002). There is also evidence for a relatively small equatorial Pacific zonal SST gradient
589 from ~900 to 1150 CE (Rustic et al., 2015), consistent with increased ENSO activity, though
590 other work suggests an increase in the zonal SST gradient (Conroy et al., 2010; Conroy et al.,
591 2009; Oppo et al., 2009; Rustic et al., 2015).

592 A southward shift of the ITCZ through the MWP could have caused drying at WI, and
593 has been inferred from the wt.-% of titanium in Cariaco Basin sediments, which declined from a
594 Medieval high of 0.24% in 947 CE to near a Medieval low of 0.14% in 1262 CE (**Fig. 7I**).
595 Climate models and theory imply that the ITCZ shifts south when the NH cools relative to the
596 SH (Schneider et al., 2014), as occurred during the first half of the MWP (Mann et al., 2008)
597 (**Fig. 7J**). However, unlike the Cariaco record, a global compilation of 25 speleothem, sediment,
598 tree ring, and ice core records sensitive to ITCZ position, merged into an ITCZ stack by

599 Lechleitner et al. (2017), averages 0.06 ± 0.2 standard units and shows no trend in ITCZ position
600 from 950-1250 CE (Lechleitner et al., 2017). Since the Cariaco wt.-% Ti record is a proxy for
601 runoff from Venezuelan Rivers, it is likely sensitive to changes in the strength of the South
602 American Monsoon that could presumably occur independent of meridional changes in central
603 Pacific ITCZ position. Barring a southward shift of the ITCZ 950-1250 CE, either or both an
604 expansion of its latitudinal range or a diminishment of tradewind convergence might also have
605 caused drying at WI, though paleoclimate evidence bearing on these possibilities is lacking.
606 Volcanoes represent another forcing mechanism of hydroclimate change in the central
607 tropical North Pacific. CMIP5 models produce significant drying in wet tropical regions in
608 response to aerosol loading of the atmosphere following volcanic eruptions (Iles and Hegerl,
609 2014). Whether they occur in northern, southern, or tropical latitudes, volcanic eruptions cause
610 zonal mean drying at the latitude of WI (5°N), with the effect particularly strong for eruptions in
611 the tropics and SH (Colose et al., 2016; PAGES-Hydro2k-Consortium, 2017). Six of the 40
612 largest eruptions of the last 2,500 yr occurred between 1100-1300 CE, all in the tropics,
613 according to a comprehensive ice-core-based reconstruction by Sigl et al. (2015) (**Fig. 7C**).
614 Notwithstanding the difficulty climate models have accurately reproducing tropical rainfall
615 patterns (which stems from the parameterizations required to simulate the small spatial-scale
616 processes of convection and cloud physics (Stephens et al., 2010)), there appears to be robust
617 drying of the central tropical North Pacific in the vicinity of WI in response to tropical eruptions
618 (Colose et al., 2016).
619 The most plausible mechanism causing drying of WI during the MWP therefore seems to
620 be the large number of large volcanic eruptions that occurred in tropical latitudes during that
621 time (Sigl et al., 2015). El Niño frequency appears to have been high at that time (Conroy et al.,
622 2010), which is expected to cause greater precipitation at WI, not less, and while the ITCZ may
623 have shifted south, as implied by the Cariaco Basin titanium record (Haug et al., 2001), other
624 records of ITCZ position don't support this (Lechleitner et al., 2017).
625
626 *4.2.2 Hydroclimate during the MWP-LIA transition: 1250-1450 CE*
627 During the transition from the MWP to the LIA (1250-1450 CE), decreases in the δ^2H
628 values of all plant, algal, and bacterial lipids in the peat sediments imply that WI became

increasingly wet (**Fig. 4B & 7B**). TLE δ^2H values in the lake sediments also declined from 1280-1390 CE, but there was little change in plant-derived fernene δ^2H values 1250-1450 CE and too few measurements of phytoplankton and bacterial lipid δ^2H values to determine any trends (**Fig. 4A, 5A**). Mechanisms that could cause WI to become increasingly wet during the MWP-LIA transition, a relatively stable period for NH (**Fig. 7J**) and global mean temperatures (Pages-2k-Consortium, 2019), include more-frequent or stronger El Niño events, a northward shift of the ITCZ, or diminished volcanism.

ENSO variance, as determined from Northern Line Islands coral $\delta^{18}O$ records (moving 30-yr standard deviation expressed as a percentage change relative to the 1961-1990 CE reference period, 5 yr time steps), was about 1/3 its 1961-1990 mean from 1250-1450 CE, declining sharply from ~1250-1350 CE and reaching its last-millennium nadir of -60% ~1370 CE (Abram et al., 2020; Cobb et al., 2003; Cobb et al., 2013; Dee et al., 2020; Grothe et al., 2019) (**Fig. 7D**). Single-foraminifera $\delta^{18}O$ analyses from near the Galápagos similarly indicate muted ENSO variance during this time (Rustic et al., 2015) (**Fig. 7E**). Both data sets are incompatible with a greater frequency or intensity of El Niño events during the MWP-LIA transition, leaving ENSO an unlikely mechanism for increased precipitation at WI. A northward shift of the ITCZ also seems unlikely to have driven the increase in precipitation, as both the Cariaco Basin titanium record (Haug et al., 2001) (**Fig. 7I**) and the multi-record ITCZ index (Lechleitner et al., 2017) were relatively trendless from 1250-1450 CE. Likewise, eruptions were relatively infrequent during the MWP-LIA transition, outside of the ~1250-1300 CE period (**Fig. 7C**), providing low or moderate volcanic forcing of WI hydroclimate (Sigl et al., 2015), and again unlikely to have driven increased precipitation.

Other potential forcings we may consider include changes in irradiance, broader-scale climate oscillations such as the North Atlantic Oscillation (NAO), or monsoon behavior. Solar forcing is a consideration during the MWP-LIA transition, as two of the most prominent minima in solar activity of the Holocene, the Wolf minimum from 1280-1350 CE and the Spörer minimum from 1415-1534 CE, occurred during that time (Eddy, 1976; Miyahara et al., 2006; Steinhilber et al., 2009). It is estimated that the radiative forcing associated with these events was -0.5 to -1.5 W m^{-2} (Steinhilber et al., 2009). However, modeling studies with GCMs that include atmospheric chemistry feedbacks imply that such a decrease in total solar irradiance is expected

659 to cause a decrease in zonal mean tropical precipitation, including in the central tropical North
660 Pacific (Shindell et al., 2006). It thus seems unlikely that solar irradiance minima ~1250-1450
661 CE can explain the apparent trend toward wetter conditions at Washington Island during that
662 time. Likewise, while positive phases of the North Atlantic Oscillation dominated from 1200-
663 1400 CE (the only such multi-decadal period of the last millennium (Ortega et al., 2015)),
664 positive phases of the NAO are only weakly associated with precipitation in the central tropical
665 Pacific, and the association is, again, opposite that needed to explain increased rainfall at WI
666 (i.e., less rainfall during NAO+) (Yu and Lin, 2016).
667 There do not appear to have been concerted changes between or within monsoon systems
668 during the transition between the MWP and LIA 1250-1450 CE. Some monsoon systems appear
669 to have strengthened 1250-1450 CE (Bird et al., 2011; Reuter et al., 2009), while others appear
670 to have weakened (Zhang et al., 2008) or shown little clear trend (Kanner et al., 2013; Novello et
671 al., 2016; Tan et al., 2011). Even within a single monsoon system, though, hydroclimate
672 reconstructions often don't agree. Within the South American Monsoon (SAM), for instance, a
673 stalagmite $\delta^{18}O$ record from Cascayunga, Peru (Reuter et al., 2009) and a sediment $\delta^{18}O$ record
674 from Lake Pumacocha, Peru (Bird et al., 2011) indicate monsoon strengthening 1250-1450 CE,
675 while stalagmite $\delta^{18}O$ records from Huagapo, Peru (Kanner et al., 2013) and Pau d'Alho, Brazil
676 (Novello et al., 2016) indicate no hydroclimate trend over this time. In the Asian Monsoon
677 system, a stalagmite $\delta^{18}O$ records from Wanxiang Cave, China (Zhang et al., 2008) indicates
678 monsoon weakening 1250-1450 CE, while another from Huangye, China (Tan et al., 2011)
679 indicates no clear trend. A lack of systematic changes in monsoon systems on either side of the
680 Pacific Ocean during the period between the MWP and LIA implies that the trend toward wetter
681 conditions at WI was unlikely to be associated with indirect effects from changes to these
682 systems.
683 The implied trend toward wetter climate conditions at Washington Island 1250-1450 CE
684 is therefore enigmatic, as it is not associated with documented changes in the position of the
685 ITCZ, ENSO variability, volcanic activity, insolation, the primary decadal-scale oscillation
686 signal at the time, or global monsoon systems. Coral $\delta^{18}O$ values from nearby Palmyra Island
687 (6°N, 162°W) were depleted by about 0.2‰ from ~1300-1475 CE relative to ~925-1225 CE,
688 implying that surface waters there were on average either fresher, warmer, or a combination of

689 the two (Cobb et al., 2003). This supports the idea that greater rainfall did indeed occur in the
690 region of Washington and Palmyra Islands during the transition between the MWP and LIA.
691 Without any clear trend in internal or external climate forcings or in large-scale climate modes
692 during the 1250-1450 CE time period, though, the implied wetting trend at WI (**Fig. 7A,B**) may
693 well have been regional or local in extent. Note that, while decreasing δ^2H values of lipid
694 biomarkers imply a trend toward wetter climatic conditions, even at its wettest the period
695 between the MWP and LIA, WI was likely drier than its modern climate since all plant
696 (sitostanol, fernene), algal (dinosterol, dinostanol), and bacterial (hop-21-ene) lipids in lake core-
697 top sediments and suspended particles had δ^2H values that were depleted relative to the 1250-
698 1450 CE time interval (**Fig. 4A**).
699
700 *4.2.3 Hydroclimate during the early LIA: 1450-1600 CE*
701 The driest period of the last millennium at WI was during the early LIA 1450-1600 CE
702 when the highest δ^2H values of fernene and the TLE in lake sediments occurred (**Fig. 7A**). These
703 were the only two δ^2H series that were continuous and of sufficiently high temporal resolution
704 through 1600 CE. The sediments deposited during this time consisted of a ~1m-thick microbial
705 mat rich with filamentous *Leptolyngbya* and coccoid *Aphanothece* cyanobacteria, similar to the
706 cyanobacterial mats growing in hypersaline ponds on Christmas (Kiritimati) Island, where
707 evaporation exceeds precipitation by 2 mm d^{-1}, and indicative of the presence of a hypersaline
708 lake (Sachs et al., 2009; Saenger et al., 2006). Deposition of the peat sediments either ceased
709 ~1450 CE or, more likely, they were eroded after canals were dug through the two peat bogs on
710 WI to connect the lake to the ocean (see **Fig. 1**) sometime around the early 20th century (Wester
711 et al., 1992). During the dry early LIA period at WI, the Galápagos (1°S, 89°W) became drier
712 (Nelson and Sachs, 2016) (**Fig. 7G**) and Palau (7°N, 134°E) became wetter (Richey and Sachs,
713 2016) (**Fig. 7H**). This pattern is consistent with an ITCZ located south of its modern position, an
714 interpretation made previously in studies of LIA hydroclimate in the tropical Pacific (Nelson and
715 Sachs, 2016; Newton et al., 2006; Oppo et al., 2009; Richey and Sachs, 2016; Sachs et al., 2009;
716 Tierney et al., 2010). Empirical support for an ITCZ located closer to the equator during the LIA
717 comes from the wt.-% of titanium in Cariaco Basin sediments (Haug et al., 2001) (**Fig. 7I**), $\delta^{18}O$
718 records from speleothems, ice cores and lake sediments in the South American Monsoon domain

(Kanner et al., 2013; Vuille et al., 2012), among others (Lechleitner et al., 2017). The 1450-1600 CE period was among the coldest 150 yr of the last two millennia in the northern hemisphere (Mann et al., 2008; Mann et al., 2009) (**Fig. 7J**), with the cooling attributed primarily to increased volcanism and reduced solar irradiance, and smaller contributions from lower atmospheric CO_2 and land use changes (Atwood et al., 2016). The resultant warming of the southern extratropics relative to the northern extratropics 1450-1600 CE may well have been the driver of a southward shift of the ITCZ at that time (Marcott et al., 2013; Schneider et al., 2014).

Alternatives to a southward shift of the entire Pacific ITCZ 1450-1600 CE are important to consider in light of the relatively small radiative forcing change during the LIA (Atwood et al., 2016) and the recent analysis by Atwood et al. (2020) of the tropical rainfall response to different climate forcings in a large set of CMIP3 and PMIP3/CMIP5 models. These models indicate that zonal shifts in the ITCZ vary significantly by longitude across the Pacific and that the concept of a uniform shift that spans the entire basin may not be useful (Atwood et al., 2020). Hydroclimate reconstructions from the western tropical Pacific during the LIA that support a contraction of the latitude range over which the ITCZ migrates (Denniston et al., 2016; Yan et al., 2015) rather than a southward migration of the precipitation centroid, which would be consistent with this view.

Another potential contributor to drier conditions at WI 1450-1600 CE may have been less frequent and/or weaker El Niño events. The $\delta^{18}O$ variance (single foram analysis) of planktonic foraminifera populations near the Galápagos was approximately 20% lower than modern values 1450-1600 CE, which implies a 55% lower ENSO amplitude according to Rustic et al. (2015) (**Fig. 7E**). A short 16th-century $\delta^{18}O$ series from fossil corals at nearby Palmyra and Christmas Islands also shows low variance during this time compared to the 1961-1990 mean (Abram et al., 2020; Cobb et al., 2003; Cobb et al., 2013; Dee et al., 2020; Grothe et al., 2019), implying reduced ENSO variability (**Fig. 7D**). Since El Niño events are associated with substantially greater rainfall at WI, fewer such events over several decades may have resulted in less annualized mean rainfall during the period. La Niña events, which are associated with diminished rainfall at WI, do not appear to have been stronger or more frequent, based on a variety of proxies of lipid biomarker, isotopic, and sedimentological proxies of rainfall in the Galápagos (Atwood and Sachs, 2014; Conroy et al., 2008; Zhang et al., 2014) and nearby single foraminifera $\delta^{18}O$ data (Rustic et al., 2015). A strong zonal SST gradient across the tropical

749 Pacific during this time, however, is indicative of a La Niña-like mean state (Rustic et al., 2015)
750 (**Fig. 7F**). We thus propose that less frequent and/or weaker El Niño events and a more La Niña-
751 like mean state in the tropical Pacific contributed to drier conditions at WI 1450-1600 CE.
752
753 *4.2.4 Hydroclimate since 1600 CE*
754 The modern hydroclimate regime was likely established at WI by ~1650 CE, as
755 evidenced by δ^2H values of phytoplankton (dinostanol, dinosterol), vascular plant (sitostanol),
756 and microbial (hop-21-ene) lipids that approached their respective core-top and suspended-
757 particulate values at that time (**Fig. 4A**). Historical accounts indicate that the modern freshwater
758 lake that exists today was in place by 1798 CE (Wester et al., 1992). The 30-70‰ decrease in the
759 δ^2H values of hop-21-ene and the TLE (both equivalent to 2 standard units; **Fig. 5A**) places the
760 climate transition from arid Christmas-Island-like conditions (896 mm yr^{-1}) to wet modern-like
761 conditions (2,903 mm yr^{-1}) (Sachs et al., 2009; Saenger et al., 2006) at about 1600-1640 CE.
762 This transition could have resulted from a northward shift of the ITCZ, since WI receives
763 41% of its rainfall in May-July (ITCZ north) compared to 11% in January-March (ITCZ south)
764 (Adler et al., 2018), a scenario supported by a century-long wet phase in Palau (**Fig. 7H**) and a
765 century of higher titanium concentrations in Cariaco Basin sediments (both ~1550-1650 CE)
766 (**Fig. 7I**). However, such a shift would be expected to cause drying in the Galápagos, but there is
767 no indication of a transition to more arid conditions in algal lipid δ^2H records from the
768 Galápagos highlands (Atwood and Sachs, 2014; Sachs et al., 2009) or lowlands (Nelson and
769 Sachs, 2016) during this time. Reconstructed water δ^2H values in Diablas Lake, Galápagos, in
770 fact, similarly show a transition from high to low values 1550-1650 CE, indicating a transition
771 from a drier to wetter climate (Nelson and Sachs, 2016).
772 Alternatively, changes in ENSO may have caused the transition from dry to wet
773 conditions at WI ~1600-1650 CE. The 17th century was characterized by the highest ENSO (**Fig.**
774 **7D**) and Indian Ocean Dipole (IOD) variability of the last millennium, based on coral $\delta^{18}O$, with
775 a particularly high proportion of central Pacific (CP) events relative to eastern Pacific (EP)
776 events (Abram et al., 2020; Cobb et al., 2003; Cobb et al., 2013; Dee et al., 2020; Freund et al.,
777 2019; Grothe et al., 2019). Wetter climate conditions at WI occur during El Niño (**Fig. 6D**), and
778 a greater proportion of CP events may have contributed to this pattern. Furthermore, a clear

779 transition from low to high $\delta^{18}O$ variance in single foraminifera near the Galápagos occurred
780 ~1600 CE, consistent with a transition to greater ENSO variability and more frequent El Niño
781 events (Rustic et al., 2015), as well as the wetter climate described by Nelson and Sachs (2016)
782 (**Fig. 7E,G**). The 17th century was characterized by the smallest zonal SST gradient across the
783 tropical Pacific of the last millennium (**Fig. 7F**), an El Niño-like mean state that may be
784 conducive to enhanced ENSO variability (Freund et al., 2019; Rustic et al., 2015).
785 Neither volcanoes nor solar forcing seem to have contributed appreciably to the
786 increasing precipitation at WI 1600-1650 CE. Three of the 40 largest eruptions of the last 2,500
787 yr occurred between 1600-1650 CE, all in the tropics (Sigl et al., 2015) (**Fig. 7C**). Since tropical
788 eruptions tend to cause drying in the latitude band of WI (Colose et al., 2016; PAGES-Hydro2k-
789 Consortium, 2017) these events appear not to have dominated the precipitation regime at WI
790 during that time. Neither does insolation, as globally averaged total solar irradiance was near its
791 late Holocene average for the 1600-1650 CE period that occurred between the Spörer and
792 Maunder minima (Steinhilber et al., 2009; Vieira et al., 2011).
793
794 **5. Conclusion**
795 The hydrogen isotope composition of triterpenoid lipids diagnostic of plants, microalgae,
796 and bacteria were measured in sediments from a peat bog and a lake on Washington Island (5°N,
797 160°W) in the central tropical North Pacific Ocean to reconstruct hydroclimate variations during
798 the last millennium. Increasing $\delta^{2}H$ values of these lipids in Washington Lake sediments indicate
799 a drying trend during the Medieval Warm Period (900-1250 CE). This drying is hypothesized to
800 have been driven by extensive volcanism in northern, southern, and tropical latitudes, all of
801 which tend to cause zonal mean drying at the latitude of WI (5°N). From 1250-1450 CE, $\delta^{2}H$
802 values of plant and microbial lipids in peat sediments decreased, signaling a trend toward wetter
803 climate conditions. Because this trend did not coincide with any trend in internal or external
804 climate forcings (i.e., ITCZ, ENSO, volcanoes, solar insolation, monsoons) it may well have
805 been regional or local in extent. A 0.2‰ lowering of coral $\delta^{18}O$ values from nearby Palmyra
806 Island ~1300-1475 CE relative to ~925-1225 CE, which would be expected to occur if
807 precipitation was appreciably higher, is consistent with this possibility. The driest period of the
808 last millennium at WI occurred ~1450-1600 CE and may have been caused by an ITCZ located

809 south of its modern position, less frequent and/or weaker El Niño events, and/or a La Niña-like
810 mean state in the tropical Pacific. The transition from early LIA dry conditions to wet modern-
811 like conditions at WI ~1600-1650 CE is hypothesized to have been caused by increased ENSO
812 variability, frequent central Pacific El Niños relative to EP El Niños, and a decline in the zonal
813 SST gradient across the tropical Pacific reflecting an El Niño-like mean state.
814 Because rainfall, not temperature, represents the primary mode of climate variation in the
815 tropics, a clear need exists for last-millennium hydroclimate reconstructions in the tropical
816 Pacific that are minimally impacted by monsoon circulations. This study provides one such
817 record from the central equatorial North Pacific. Additional hydroclimate reconstructions are
818 needed to characterize with confidence the natural patterns of rainfall across the vast tropical
819 Pacific Ocean during the millennium preceding widespread anthropogenic emissions of
820 greenhouse gases, and what may have caused them.
821
822 **Acknowledgements**
823 This material is based upon work supported by the U.S. National Science Foundation under
824 grants NSF-EAR-0823503 (J.P.S.) and NSF-ESH-0639640 (J.P.S.), and by the U.S. National
825 Oceanic and Atmospheric Administration under NOAA Grant No. 08OAR4310685 (J.P.S.). The
826 Alexander von Humboldt Foundation is acknowledged for proving a Feodor-Lynen Research
827 Fellowship to Ines Mügler. We thank Rienk H. Smittenberg, Casey Saenger, and Michael Miller
828 for their assistance in the field. We are grateful to Orest Kawka and Alyssa Atwood at the
829 University of Washington for their technical assistance and discussions. Fieldwork on
830 Washington Island was conducted with the support and permission of the Kiribati Ministry of
831 Environment and Natural Resources Development and the Kiritimati Ministers of the
832 Environment and Fisheries. We wish to thank the Parliament of Teraina for their hospitality
833 while hosting us. We are grateful for the thoughtful comments and reviews of the editors and two
834 anonymous reviewers which helped to improve this manuscript.
835
836 **References**
837
838 Abram, N.J., Wright, N.M., Ellis, B., Dixon, B.C., Wurtzel, J.B., England, M.H., Ummenhofer, C.C.,
839 Philibosian, B., Cahyarini, S.Y., Yu, T.-L., Shen, C.-C., Cheng, H., Edwards, R.L. and Heslop, D.

(2020) Coupling of Indo-Pacific climate variability over the last millennium. Nature 579, 385-392.
Adler, R., Sapiano, M., Huffman, G., Wang, J.-J., Gu, G., Bolvin, D., Chiu, L., Schneider, U., Becker, A., Nelkin, E., Xie, P., Ferraro, R. and Shin, D.-B. (2018) The Global Precipitation Climatology Project (GPCP) Monthly Analysis (New Version 2.3) and a Review of 2017 Global Precipitation. Atmosphere 9, 138.
Ageta, H. and Arai, Y. (1983) Fern constituents: pentacyclic triterpenoids isolated from Polypodium niponicum and P. formosanum. Phytochemistry 22, 1801-1808.
Ageta, H., Iwata, K. and Natori, S. (1963) A fern constituent, fernene a triterpenoid hydrocarbon of a new type. Tetrahedron Letters 4, 1447-1450.
Ahmed, M., Anchukaitis, K.J., Asrat, A., Borgaonkar, H.P., Braida, M., Buckley, B.M., Büntgen, U., Chase, B.M., Christie, D.A., Cook, E.R., Curran, M.A.J., Diaz, H.F., Esper, J., Fan, Z.-X., Gaire, N.P., Ge, Q., Gergis, J., González-Rouco, J.F., Goosse, H., Grab, S.W., Graham, N., Graham, R., Grosjean, M., Hanhijärvi, S.T., Kaufman, D.S., Kiefer, T., Kimura, K., Korhola, A.A., Krusic, P.J., Lara, A., Lézine, A.-M., Ljungqvist, F.C., Lorrey, A.M., Luterbacher, J., Masson-Delmotte, V., McCarroll, D., McConnell, J.R., McKay, N.P., Morales, M.S., Moy, A.D., Mulvaney, R., Mundo, I.A., Nakatsuka, T., Nash, D.J., Neukom, R., Nicholson, S.E., Oerter, H., Palmer, J.G., Phipps, S.J., Prieto, M.R., Rivera, A., Sano, M., Severi, M., Shanahan, T.M., Shao, X., Shi, F., Sigl, M., Smerdon, J.E., Solomina, O.N., Steig, E.J., Stenni, B., Thamban, M., Trouet, V., Turney, C.S.M., Umer, M., van Ommen, T., Verschuren, D., Viau, A.E., Villalba, R., Vinther, B.M., von Gunten, L., Wagner, S., Wahl, E.R., Wanner, H., Werner, J.P., White, J.W.C., Yasue, K. and Zorita, E. (2013) Continental-scale temperature variability during the past two millennia. Nature Geoscience 6, 339.
Anderson, C., Fuller, F. and Epstein, W.W. (1979) Nonpolar Pentacyclic Triterpenes of the Medicinal Fern Polypodium subpetiolatum. J Nat Prod 42, 168-173.
Atwood, A.R., Donohoe, A., Battisti, D.S., Liu, X. and Pausata, F.S.R. (2020) Robust longitudinally-variable responses of the ITCZ to a myriad of climate forcings. Geophys Res Lett 47, e2020GL088833.
Atwood, A.R. and Sachs, J.P. (2012) Purification of dinosterol from complex mixtures of sedimentary lipids for hydrogen isotope analysis. Organic Geochemistry 48, 37-46.
Atwood, A.R. and Sachs, J.P. (2014) Separating ITCZ- and ENSO-related rainfall changes in the Galapagos over the last 3 kyr using D/H ratios of multiple lipid biomarkers. Earth and Planetary Science Letters 404, 408-419.
Atwood, A.R., Volkman, J.K. and Sachs, J.P. (2014) Characterization of unusual sterols and long chain diols, triols, keto-ols and n-alkenols in El Junco Lake, Galapagos. Organic Geochemistry 66, 80-89.
Atwood, A.R., Wu, E., Frierson, D.M.W., Battisti, D.S. and Sachs, J.P. (2016) Quantifying Climate Forcings and Feedbacks over the Last Millennium in the CMIP5–PMIP3 Models. Journal of Climate 29, 1161-1178.
Belin, B.J., Busset, N., Giraud, E., Molinaro, A., Silipo, A. and Newman, D.K. (2018) Hopanoid lipids: from membranes to plant–bacteria interactions. Nature Reviews Microbiology 16, 304-315.
Bird, B.W., Abbott, M.B., Vuille, M., Rodbell, D.T., Stansell, N.D. and Rosenmeier, M.F. (2011) A 2,300-year-long annually resolved record of the South American summer monsoon from the Peruvian Andes. Proceedings of the National Academy of Sciences 108, 8583-8588.
Blaauw, M. and Christen, J.A. (2011) Flexible paleoclimate age-depth models using an autoregressive gamma process. Bayesian Analysis 6, 457-474.
Boon, J.J., Rijpstra, W.I.C., De Lange, F., De Leeuw, J.W., Yoshioka, M. and Shimizu, Y. (1979) Black Sea sterol—a molecular fossil for dinoflagellate blooms. Nature 277, 125-127.
Bottari, F., Marsili, A., Morelli, I. and Pacchiani, M. (1972) Aliphatic and triterpenoid hydrocarbons from ferns. Phytochemistry 11, 2519-2523.

Bowen, G.J. (2017) The Online Isotopes in Precipitation Calculator, version 3.1. http://www.waterisotopes.org.
Bowen, G.J. and Revenaugh, J. (2003) Interpolating the isotopic composition of modern meteoric precipitation. Water Resources Research 39, 1299.
Chikaraishi, Y. and Naraoka, H. (2005) δ13C and δD identification of sources of lipid biomarkers in sediments of Lake Haruna (Japan). Geochimica et Cosmochimica Acta 69, 3285-3297.
Chikaraishi, Y., Naraoka, H. and Poulson, S.R. (2004) Carbon and hydrogen isotopic fractionation during lipid biosynthesis in a higher plant (Cryptomeria japonica). Phytochemistry 65, 323-330.
Chivall, D., M'Boule, D., Sinke-Schoen, D., Sinninghe Damsté, J.S., Schouten, S. and van der Meer, M.T.J. (2014) The effects of growth phase and salinity on the hydrogen isotopic composition of alkenones produced by coastal haptophyte algae. Geochimica et Cosmochimica Acta 140, 381-390.
Cobb, K.M., Charles, C.D., Cheng, H. and Edwards, R.L. (2003) El Niño/Southern Oscillation and tropicalPacific climate during the last millennium. Nature 424, 271-276.
Cobb, K.M., Westphal, N., Sayani, H.R., Watson, J.T., Di Lorenzo, E., Cheng, H., Edwards, R.L. and Charles, C.D. (2013) Highly Variable El Niño–Southern Oscillation Throughout the Holocene. Science 339, 67-70.
Colose, C.M., LeGrande, A.N. and Vuille, M. (2016) Hemispherically asymmetric volcanic forcing of tropical hydroclimate during the last millennium. Earth Syst. Dynam. 7, 681-696.
Conroy, J.L., Overpeck, J.T. and Cole, J.E. (2010) El Niño/Southern Oscillation and changes in the zonal gradient of tropical Pacific sea surface temperature over the last 1.2 ka. PAGES news 18, 32-34.
Conroy, J.L., Overpeck, J.T., Cole, J.E., Shanahan, T.M. and Steinitz-Kannan, M. (2008) Holocene changes in eastern tropical Pacific climate inferred from a Galápagos lake sediment record. Quaternary Science Reviews 27, 1166-1180.
Conroy, J.L., Restrepo, A., Overpeck, J.T., Steinitz-Kannan, M., Cole, J.E., Bush, M.B. and Colinvaux, P.A. (2009) Unprecedented recent warming of surface temperatures in the eastern tropical Pacific Ocean. Nature Geosci 2, 46-50.
Crowley, T.J. (2000) Causes of Climate Change Over the Past 1000 Years. Science 289, 270-277.
Dansgaard, W. (1964) Stable isotopes in precipitation. Tellus 16, 436-447.
Dee, S.G., Cobb, K.M., Emile-Geay, J., Ault, T.R., Edwards, R.L., Cheng, H. and Charles, C.D. (2020) No consistent ENSO response to volcanic forcing over the last millennium. Science 367, 1477-1481.
Denniston, R.F., Ummenhofer, C.C., Wanamaker, A.D., Lachniet, M.S., Villarini, G., Asmerom, Y., Polyak, V.J., Passaro, K.J., Cugley, J., Woods, D. and Humphreys, W.F. (2016) Expansion and Contraction of the Indo-Pacific Tropical Rain Belt over the Last Three Millennia. Scientific Reports 6, 34485.
Douka, E., Koukkou, A.-I., Drainas, C., Grosdemange-Billiard, C. and Rohmer, M. (2001) Structural diversity of the triterpenic hydrocarbons from the bacterium Zymomonas mobilis: the signature of defective squalene cyclization by the squalene/hopene cyclase. FEMS Microbiology Letters 199, 247-251.
Eddy, J.A. (1976) The Maunder Minimum. Science 192, 1189-1202.
Elvert, M., Whiticar, M.J. and Suess, E. (2001) Diploptene in varved sediments of Saanich Inlet: indicator of increasing bacterial activity under anaerobic conditions during the Holocene. Marine Geology 174, 371-383.
Englebrecht, A.C. and Sachs, J.P. (2005) Determination of sediment provenance at drift sites using hydrogen isotopes and unsaturation ratios in alkenones. Geochimica et Cosmochimica Acta 69, 4253-4265.
Feakins, S. and Sessions, A.L. (2010) Controls on the D/H ratios of plant leaf waxes from an arid ecosystem. Geochimica Et Cosmochimica Acta 74, 2128-2141.

939 Freeman, K.H., Hayes, J.M., Trendel, J.M. and Albrecht, P. (1990) Evidence from Carbon Isotope
940 Measurements for Diverse Origins of Sedimentary Hydrocarbons. Nature 343, 254-256.
941 Freund, M.B., Henley, B.J., Karoly, D.J., McGregor, H.V., Abram, N.J. and Dommenget, D. (2019)
942 Higher frequency of Central Pacific El Niño events in recent decades relative to past centuries.
943 Nature Geoscience 12, 450-455.
944 Gaskell, S.J. and Eglinton, G. (1975) Rapid hydrogenation of sterols in a contemporary lacustrine
945 sediment. Nature 254, 209-211.
946 Gaskell, S.J. and Eglinton, G. (1976) Sterols of a contemporary lacustrine sediment. Geochimica et
947 Cosmochimica Acta 40, 1221-1228.
948 Goad, L. and Goodwin, T. (1972) Biosynthesis of plant sterols. Progr Phytochem.
949 Gould, J., Kienast, M., Dowd, M. and Schefuß, E. (2019) An open-ocean assessment of alkenone δD as a
950 paleo-salinity proxy. Geochimica et Cosmochimica Acta 246, 478-497.
951 Grothe, P.R., Cobb, K.M., Liguori, G., Di Lorenzo, E., Capotondi, A., Lu, Y., Cheng, H., Edwards, R.L.,
952 Southon, J.R., Santos, G.M., Deocampo, D.M., Lynch-Stieglitz, J., Chen, T., Sayani, H.R.,
953 Thompson, D.M., Conroy, J.L., Moore, A.L., Townsend, K., Hagos, M., O'Connor, G. and Toth,
954 L.T. (2019) Enhanced El Niño–Southern Oscillation Variability in Recent Decades. Geophys Res
955 Lett 47, e2019GL083906.
956 Grunwald, C. (1975) Plant sterols. Annual review of plant physiology 26, 209-236.
957 Hanisch, S., Ariztegui, D. and Puttmann, W. (2003) The biomarker record of Lake Albano, central Italy -
958 implications for Holocene aquatic system response to environmental change. Organic
959 Geochemistry 34, 1223-1235.
960 Härtner, T., Straub, K.L. and Kannenberg, E. (2005) Occurrence of hopanoid lipids in anaerobic
961 Geobacter species. FEMS Microbiology Letters 243, 59-64.
962 Haug, G.H., Hughen, K.A., Sigman, D.M., Peterson, L.C. and Rohl, U. (2001) Southward Migration of
963 the Intertropical Convergence Zone Through the Holocene. Science 293, 1304-1308.
964 Hefter, J., Thiel, V., Jenisch, A., Galling, U., Kempe, S. and Michaelis, W. (1993) Biomarker indications
965 for microbial contribution to Recent and Late Jurassic carbonate deposits. Facies 29, 93-105.
966 Heinzelmann, S.M., Chivall, D., M'Boule, D., Sinke-Schoen, D., Villanueva, L., Damsté, J.S.S.,
967 Schouten, S. and van der Meer, M.T.J. (2015) Comparison of the effect of salinity on the D/H
968 ratio of fatty acids of heterotrophic and photoautotrophic microorganisms. FEMS Microbiology
969 Letters 362, fnv065.
970 Howard, D.L., Simoneit, B.R.T. and Chapman, D.J. (1984) Triterpenoids from lipids of Rhodomicrobium
971 vanniellii. Arch Microbiol 137, 200-204.
972 Huang, W.-Y. and Meinschein, W.G. (1979) Sterols as ecological indicators. Geochimica et
973 Cosmochimica Acta 43, 739-745.
974 Huang, X., Wang, C., Xue, J., Meyers, P.A., Zhang, Z., Tan, K., Zhang, Z. and Xie, S. (2010) Occurrence
975 of diploptene in moss species from the Dajiuhu Peatland in southern China. Organic
976 Geochemistry 41, 321-324.
977 Huang, Y.S., Shuman, B., Wang, Y. and Webb, T. (2004) Hydrogen isotope ratios of individual lipids in
978 lake sediments as novel tracers of climatic and environmental change: a surface sediment test.
979 Journal of Paleolimnology 31, 363-375.
980 IAEA/WMO (2015) Global Network of Isotopes in Precipitation. The GNIP Database.
981 Iles, C.E. and Hegerl, G.C. (2014) The global precipitation response to volcanic eruptions in the CMIP5
982 models. Environmental Research Letters 9, 104012.
983 Inayama, S., Hori, H., Pang, G.-M., Nagasawa, H. and Ageta, H. (1989) Isolation of a Hopane-Type
984 Triterpenoid, Zeorin, from a Higher Plant, Tripterygium regelii. CHEMICAL &
985 PHARMACEUTICAL BULLETIN 37, 2836-2837.
986 Kahmen, A., Hoffmann, B., Schefuß, E., Arndt, S.K., Cernusak, L.A., West, J.B. and Sachse, D. (2013)
987 Leaf water deuterium enrichment shapes leaf wax n-alkane δD values of angiosperm plants II:
988 Observational evidence and global implications. Geochimica et Cosmochimica Acta 111, 50-63.

Kaiser, J., Ön, B., Arz, H.W. and Akçer-Ön, S. (2016) Sedimentary lipid biomarkers in the magnesium rich and highly alkaline Lake Salda (south-western Anatolia). Journal of limnology 75.
Kannenberg, E.L. and Poralla, K. (1999) Hopanoid Biosynthesis and Function in Bacteria. Naturwissenschaften 86, 168-176.
Kanner, L.C., Burns, S.J., Cheng, H., Edwards, R.L. and Vuille, M. (2013) High-resolution variability of the South American summer monsoon over the last seven millennia: insights from a speleothem record from the central Peruvian Andes. Quaternary Science Reviews 75, 1-10.
Kurita, N., Ichiyanagi, K., Matsumoto, J., Yamanaka, M.D. and Ohata, T. (2009) The relationship between the isotopic content of precipitation and the precipitation amount in tropical regions. Journal of Geochemical Exploration 102, 113-122.
Ladd, S.N. and Sachs, J.P. (2015a) Hydrogen isotope response to changing salinity and rainfall in Australian mangroves. Plant, Cell & Environment 38, 2674-2687.
Ladd, S.N. and Sachs, J.P. (2015b) Influence of salinity on hydrogen isotope fractionation in Rhizophora mangroves from Micronesia. Geochimica et Cosmochimica Acta 168, 206-221.
Lamb, H.H. (1965) The early medieval warm epoch and its sequel. Palaeogeography, Palaeoclimatology, Palaeoecology 1, 13-37.
Leblond, J.D. and Chapman, P.J. (2002) A survey of the sterol composition of the marine dinoflagellates Karenia brevis, Karenia mikimotoi, and Karlodinium micrum distribution of sterols within other members of the class Dinophyceae. Journal of Phycology 38, 670-682.
Lechleitner, F.A., Breitenbach, S.F.M., Rehfeld, K., Ridley, H.E., Asmerom, Y., Prufer, K.M., Marwan, N., Goswami, B., Kennett, D.J., Aquino, V.V., Polyak, V., Haug, G.H., Eglinton, T.I. and Baldini, J.U.L. (2017) Tropical rainfall over the last two millennia: evidence for a low-latitude hydrologic seesaw. Scientific Reports 7, 45809.
Lee, J.-E. and Fung, I. (2008) "Amount effect" of water isotopes and quantitative analysis of post-condensation processes. Hydrological Processes 22, 1-8.
M'boule, D., Chivall, D., Sinke-Schoen, D., Sinninghe Damsté, J.S., Schouten, S. and van der Meer, M.T.J. (2014) Salinity dependent hydrogen isotope fractionation in alkenones produced by coastal and open ocean haptophyte algae. Geochimica et Cosmochimica Acta 130, 126-135.
Maloney, A.E., Shinneman, A.L.C., Hemeon, K. and Sachs, J.P. (2016) Exploring lipid 2H/1H fractionation mechanisms in response to salinity with continuous cultures of the diatom Thalassiosira pseudonana. Organic Geochemistry 101, 154-165.
Mann, M.E., Zhang, Z., Hughes, M.K., Bradley, R.S., Miller, S.K., Rutherford, S. and Ni, F. (2008) Proxy-based reconstructions of hemispheric and global surface temperature variations over the past two millennia. Proceedings of the National Academy of Sciences 105, 13252-13257.
Mann, M.E., Zhang, Z., Rutherford, S., Bradley, R.S., Hughes, M.K., Shindell, D., Ammann, C., Faluvegi, G. and Ni, F. (2009) Global Signatures and Dynamical Origins of the Little Ice Age and Medieval Climate Anomaly. Science 326, 1256-1260.
Marcott, S.A., Shakun, J.D., Clark, P.U. and Mix, A.C. (2013) A Reconstruction of Regional and Global Temperature for the Past 11,300 Years. Science 339, 1198-1201.
Miyahara, H., Masuda, K., Muraki, Y., Kitagawa, H. and Nakamura, T. (2006) Variation of solar cyclicity during the Spoerer Minimum. Journal of Geophysical Research: Space Physics 111.
Moy, C.M., Seltzer, G.O., Rodbell, D.T. and Anderson, D.M. (2002) Variability of El Nino/Southern Oscillation activity at millennial timescales during the Holocene epoch. Nature 420, 162-165.
Nelson, D.B. and Sachs, J.P. (2013) Concurrent purification of sterols, triterpenols and alkenones from sediments for hydrogen isotope analysis using high performance liquid chromatography. Organic Geochemistry 64, 19-28.
Nelson, D.B. and Sachs, J.P. (2014a) The influence of salinity on D/H fractionation in alkenones from saline and hypersaline lakes in continental North America. Organic Geochemistry 66, 38-47.

Nelson, D.B. and Sachs, J.P. (2014b) The influence of salinity on D/H fractionation in dinosterol and brassicasterol from globally distributed saline and hypersaline lakes. Geochimica Et Cosmochimica Acta 133, 325-339.
Nelson, D.B. and Sachs, J.P. (2016) Galápagos hydroclimate of the Common Era from paired microalgal and mangrove biomarker 2H/1H values. Proceedings of the National Academy of Sciences 113, 3476-3481.
Newton, A., Thunell, R. and Stott, L. (2006) Climate and hydrographic variability in the Indo-Pacific Warm Pool during the last millennium. Geophys Res Lett 33, L19710.
Nishimura, M. (1978) Geochemical characteristics of the high reduction zone of stenols in Suwa sediments and the environmental factors controlling the conversion of stenols into stanols. Geochimica et Cosmochimica Acta 42, 349-357.
Nishimura, M. and Koyama, T. (1976) Stenols and stanols in lake sediments and diatoms. Chemical Geology 17, 229-239.
Novello, V.F., Vuille, M., Cruz, F.W., Stríkis, N.M., de Paula, M.S., Edwards, R.L., Cheng, H., Karmann, I., Jaqueto, P.F., Trindade, R.I.F., Hartmann, G.A. and Moquet, J.S. (2016) Centennial-scale solar forcing of the South American Monsoon System recorded in stalagmites. Scientific Reports 6, 24762.
Oppo, D.W., Rosenthal, Y. and Linsley, B.K. (2009) 2,000-year-long temperature and hydrology reconstructions from the Indo-Pacific warm pool. Nature 460, 1113-1116.
Ortega, P., Lehner, F., Swingedouw, D., Masson-Delmotte, V., Raible, C.C., Casado, M. and Yiou, P. (2015) A model-tested North Atlantic Oscillation reconstruction for the past millennium. Nature 523, 71-74.
Ourisson, G., Albrecht, P. and Rohmer, M. (1979) The Hopanoids: Palaeochemistry and Biochemistry of a Group of Natural Products. Pure Appl Chem 51, 709-729.
Ourisson, G., Rohmer, M. and Poralla, K. (1987) Prokaryotic hopanoids and other polyterpenoid sterol surrogates. Annual Reviews in Microbiology 41, 301-333.
Pages-2k-Consortium (2019) Consistent multi-decadal variability in global temperature reconstructions and simulations over the Common Era. Nat Geosci 12, 643-649.
PAGES-Hydro2k-Consortium (2017) Comparing proxy and model estimates of hydroclimate variability and change over the Common Era. Clim. Past 13, 1851-1900.
Piretti, M.V., Pagliuca, G., Boni, L., Pistocchi, R., Diamante, M. and Gazzotti, T. (1997) Investigation of 4-methyl sterols from cultured dinoflagellate algal strains. Journal of Phycology 33, 61-67.
Prahl, F.G., Hayes, J.M. and Xie, T.-M. (1992) Diploptene: An Indicator of terrigenous organic carbon in Washington coastal sediments. Limnology and Oceanography 37, 1290-1299.
Reimer, P.J., Bard, E., Bayliss, A., Beck, J.W., Blackwell, P.G., Ramsey, C.B., Buck, C.E., Cheng, H., Edwards, R.L., Friedrich, M., Grootes, P.M., Guilderson, T.P., Haflidason, H., Hajdas, I., Hatté, C., Heaton, T.J., Hoffmann, D.L., Hogg, A.G., Hughen, K.A., Kaiser, K.F., Kromer, B., Manning, S.W., Niu, M., Reimer, R.W., Richards, D.A., Scott, E.M., Southon, J.R., Staff, R.A., Turney, C.S.M. and van der Plicht, J. (2013) IntCal13 and Marine13 Radiocarbon Age Calibration Curves 0–50,000 Years cal BP. Radiocarbon 55, 1869-1887.
Reuter, J., Stott, L., Khider, D., Sinha, A., Cheng, H. and Edwards, R.L. (2009) A new perspective on the hydroclimate variability in northern South America during the Little Ice Age. Geophys Res Lett 36, n/a-n/a.
Richey, J.N. and Sachs, J.P. (2016) Precipitation changes in the western tropical Pacific over the past millennium. Geology 44, 671-674.
Ries-Kautt, M. and Albrecht, P. (1989) Hopane-derived triterpenoids in soils. Chemical Geology 76, 143-151.
Risi, C., Bony, S. and Vimeux, F. (2008) Influence of convective processes on the isotopic composition (δ18O andδD) of precipitation and water vapor in the tropics: 2. Physical interpretation of the amount effect. Journal of Geophysical Research 113.

1087 Robinson, N., Eglinton, G., Brassell, S.C. and Cranwell, P.A. (1984) Dinoflagellate origin for
1088 sedimentary 4[alpha]-methylsteroids and 5[alpha](H)-stanols. Nature 308, 439-442.
1089 Rohmer, M., Bisseret, P. and Neunlist, S. (1992) The hopanoids, prokaryotic triterpenoids and precursors
1090 of ubiquitous molecular fossils. Prentice Hall Englewood Cliffs, NJ, pp. 1-17.
1091 Rohmer, M., Bouviernave, P. and Ourisson, G. (1984) Distribution of Hopanoid Triterpenes in
1092 Prokaryotes. J Gen Microbiol 130, 1137-1150.
1093 Rozanski, K., Araguas-Araguas, L. and Gonfiantini, R. (1993) Isotopic patterns in modem global
1094 precipitation, in: Swart, P.K., Lohman, K.C., McKenzie, J., Savin, S. (Eds.), Climate Change in
1095 Continental Isotopic Records - Geophysical Monograph 78. American Geophysical Union,
1096 Washington, D.C., pp. 1-36.
1097 Rustic, G.T., Koutavas, A., Marchitto, T.M. and Linsley, B.K. (2015) Dynamical excitation of the tropical
1098 Pacific Ocean and ENSO variability by Little Ice Age cooling. Science 350, 1537-1541.
1099 Sachs, J.P., Blois, J., McGee, T., Wolhowe, M., Haberle, S., Clark, G. and Atahan, P. (2018a) Southward
1100 Shift of the Pacific ITCZ During the Holocene. Paleoceanography and Paleoclimatology
1101 Accepted.
1102 Sachs, J.P., Blois, J.L., McGee, T., Wolhowe, M., Haberle, S., Clark, G. and Atahan, P. (2018b)
1103 Southward Shift of the Pacific ITCZ During the Holocene. Paleoceanography and
1104 Paleoclimatology 33, 1383-1395.
1105 Sachs, J.P. and Kawka, O.E. (2015) The influence of growth rate on 2H/1H fractionation in continuous
1106 cultures of the coccolithophorid Emiliania huxleyi and the diatom Thalassiosira pseudonana.
1107 PLOS ONE 10, e0141643.
1108 Sachs, J.P., Maloney, A.E. and Gregersen, J. (2017) Effect of light on 2H/1H fractionation in lipids from
1109 continuous cultures of the diatom Thalassiosira pseudonana. Geochimica et Cosmochimica Acta
1110 209, 204-215.
1111 Sachs, J.P., Maloney, A.E., Gregersen, J. and Paschall, C. (2016) Effect of salinity on 2H/1H
1112 fractionation in lipids from continuous cultures of the coccolithophorid Emiliania huxleyi.
1113 Geochimica et Cosmochimica Acta 189, 96-109.
1114 Sachs, J.P., Sachse, D., Smittenberg, R.H., Zhang, Z., Battisti, D.S. and Golubic, S. (2009) Southward
1115 movement of the Pacific intertropical convergence zone AD 1400-1850. Nature Geoscience 2,
1116 519-525.
1117 Sachs, J.P. and Schwab, V.F. (2011) Hydrogen isotopes in dinosterol from the Chesapeake Bay estuary.
1118 Geochimica et Cosmochimica Acta 75, 444-459.
1119 Sachs, J.P., Stein, R., Maloney, A.E., Wolhowe, M., Fahl, K. and Nam, S.-i. (2018c) An Arctic Ocean
1120 paleosalinity proxy from δ2H of palmitic acid provides evidence for deglacial Mackenzie River
1121 flood events. Quaternary Science Reviews 198, 76-90.
1122 Sachse, D., Billault, I., Bowen, G.J., Chikaraishi, Y., Dawson, T.E., Feakins, S.J., Freeman, K.H., Magill,
1123 C.R., McInerney, F.A., van der Meer, M.T.J., Polissar, P., Robins, R.J., Sachs, J.P., Schmidt, H.-
1124 L., Sessions, A.L., White, J.W.C., West, J.B. and Kahmen, A. (2012) Molecular Paleohydrology:
1125 Interpreting the Hydrogen-Isotopic Composition of Lipid Biomarkers from Photosynthesizing
1126 Organisms. Annu Rev Earth Pl Sc 40, 221-249.
1127 Sachse, D., Radke, J. and Gleixner, G. (2004) Hydrogen isotope ratios of recent lacustrine sedimentary n-
1128 alkanes record modern climate variability. Geochimica et Cosmochimica Acta 68, 4877-4889.
1129 Sachse, D. and Sachs, J.P. (2008) Inverse relationship between D/H fractionation in cyanobacterial lipids
1130 and salinity in Christmas Island saline ponds. Geochimica et Cosmochimica Acta 72, 793-806.
1131 Saenger, C., Miller, M., Smittenberg, R.H. and Sachs, J.P. (2006) A physico-chemical survey of inland
1132 lakes and saline ponds: Christmas Island (Kiritimati) and Washington (Teraina) Islands, Republic
1133 of Kiribati. Saline Systems 2, 8.
1134 Sauer, P.E., Eglinton, T.I., Hayes, J.M., Schimmelmann, A. and Sessions, A.L. (2001) Compound-
1135 specific D/H ratios of lipid biomarkers from sediments as a proxy for environmental and climatic
1136 conditions. Geochimica et Cosmochimica Acta 65, 213-222.

Schneider, T., Bischoff, T. and Haug, G.H. (2014) Migrations and dynamics of the intertropical convergence zone. Nature 513, 45-53.
Schouten, S., Ossebaar, J., Schreiber, K., Kienhuis, M.V.M., Langer, G., Benthien, A. and Bijma, J. (2006) The effect of temperature, salinity and growth rate on the stable hydrogen isotopic composition of long chain alkenones produced by Emiliania huxleyi and Gephyrocapsa oceanica. Biogeosciences 3, 113-119.
Schouten, S., Rijpstra, W.I.C., Kok, M., Hopmans, E.C., Summons, R.E., Volkman, J.K. and Damste, J.S.S. (2001) Molecular organic tracers of biogeochemical processes in a saline meromictic lake (Ace Lake). Geochimica Et Cosmochimica Acta 65, 1629-1640.
Sessions, A.L., Burgoyne, T.W., Schimmelmann, A. and Hayes, J.M. (1999) Fractionation of hydrogen isotopes in lipid biosynthesis. Organic Geochemistry 30, 1193-1200.
Shindell, D.T., Faluvegi, G., Miller, R.L., Schmidt, G.A., Hansen, J.E. and Sun, S. (2006) Solar and anthropogenic forcing of tropical hydrology. Geophys Res Lett 33.
Shiojima, K. and Ageta, H. (1990) Fern Constituents : Two New Triterpenoid Hydrocarbons, Hop-16-ene and Isohop-22(29)-ene, Isolated from Davallia mariesii. Chemical & Pharmaceutical Bulletin 38, 347-349.
Sigl, M., Winstrup, M., McConnell, J.R., Welten, K.C., Plunkett, G., Ludlow, F., Büntgen, U., Caffee, M., Chellman, N., Dahl-Jensen, D., Fischer, H., Kipfstuhl, S., Kostick, C., Maselli, O.J., Mekhaldi, F., Mulvaney, R., Muscheler, R., Pasteris, D.R., Pilcher, J.R., Salzer, M., Schüpbach, S., Steffensen, J.P., Vinther, B.M. and Woodruff, T.E. (2015) Timing and climate forcing of volcanic eruptions for the past 2,500 years. Nature 523, 543-549.
Simonin, P., Jürgens, U.J. and Rohmer, M. (1996) Bacterial Triterpenoids of the Hopane Series from the Prochlorophyte Prochlorothrix Hollandica and their Intracellular Localization. Eur J Biochem 241, 865-871.
Sinninghe Damsté, J.S., Rijpstra, W.I.C., Schouten, S., Fuerst, J.A., Jetten, M.S.M. and Strous, M. (2004) The occurrence of hopanoids in planctomycetes: implications for the sedimentary biomarker record. Organic Geochemistry 35, 561-566.
Sinninghe Damsté, J.S., Schouten, S. and Volkman, J.K. (2014) C27–C30 neohop-13(18)-enes and their saturated and aromatic derivatives in sediments: Indicators for diagenesis and water column stratification. Geochimica et Cosmochimica Acta 133, 402-421.
Smittenberg, R.H. and Sachs, J.P. (2007) Purification of dinosterol for hydrogen isotopic analysis using high-performance liquid chromatography-mass spectrometry. Journal of Chromatography A 1169, 70-76.
Smittenberg, R.H., Saenger, C., Dawson, M.N. and Sachs, J.P. (2011) Compound-specific D/H ratios of the marine lakes of Palau as proxies for West Pacific Warm Pool hydrologic variability. Quaternary Science Reviews 30, 921-933.
Steinhilber, F., Beer, J. and Fröhlich, C. (2009) Total solar irradiance during the Holocene. Geophys Res Lett 36.
Stephens, G.L., L'Ecuyer, T., Forbes, R., Gettelmen, A., Golaz, J.-C., Bodas-Salcedo, A., Suzuki, K., Gabriel, P. and Haynes, J. (2010) Dreary state of precipitation in global models. Journal of Geophysical Research: Atmospheres 115.
Tan, L., Cai, Y., An, Z., Edwards, R.L., Cheng, H., Shen, C.-C. and Zhang, H. (2011) Centennial- to decadal-scale monsoon precipitation variability in the semi-humid region, northern China during the last 1860 years: Records from stalagmites in Huangye Cave. The Holocene 21, 287-296.
Tierney, J.E., Oppo, D.W., Rosenthal, Y., Russell, J.M. and Linsley, B.K. (2010) Coordinated hydrological regimes in the Indo-Pacific region during the past two millennia. Paleoceanography 25, PA1102.
Toyota, M., Masuda, K. and Asakawa, Y. (1998) Triterpenoid constituents of the moss Floribundaria aurea subsp. Nipponica. Phytochemistry 48, 297-299.

van der Meer, M.T.J., Baas, M., Rijpstra, W.I.C., Marino, G., Rohling, E.J., Sinninghe DamstÈ, J.S. and Schouten, S. (2007) Hydrogen isotopic compositions of long-chain alkenones record freshwater flooding of the Eastern Mediterranean at the onset of sapropel deposition. Earth and Planetary Science Letters 262, 594-600.
van der Meer, M.T.J., Benthien, A., French, K.L., Epping, E., Zondervan, I., Reichart, G.-J., Bijma, J., Sinninghe Damsté, J.S. and Schouten, S. (2015) Large effect of irradiance on hydrogen isotope fractionation of alkenones in Emiliania huxleyi. Geochimica et Cosmochimica Acta 160, 16-24.
van Winden, J.F., Kip, N., Reichart, G.-J., Jetten, M.S.M., Camp, H.J.M.O.d. and Damsté, J.S.S. (2010) Lipids of symbiotic methane-oxidizing bacteria in peat moss studied using stable carbon isotopic labelling. Organic Geochemistry 41, 1040-1044.
Vasiliev, I., Mezger, E.M., Lugli, S., Reichart, G.-J., Manzi, V. and Roveri, M. (2017) How dry was the Mediterranean during the Messinian salinity crisis? Palaeogeography, Palaeoclimatology, Palaeoecology 471, 120-133.
Vasiliev, I., Reichart, G.-J. and Krijgsman, W. (2013) Impact of the Messinian Salinity Crisis on Black Sea hydrology—Insights from hydrogen isotopes analysis on biomarkers. Earth and Planetary Science Letters 362, 272-282.
Vasiliev, I., Reichart, G.-J., Krijgsman, W. and Mulch, A. (2019) Black Sea rivers capture significant change in catchment-wide mean annual temperature and soil pH during the Miocene-to-Pliocene transition. Global and Planetary Change 172, 428-439.
Vieira, L.E.A., Solanki, S.K., Krivova, N.A. and Usoskin, I. (2011) Evolution of the solar irradiance during the Holocene. Astronomy & Astrophysics 531, A6.
Volkman, J. (2003) Sterols in microorganisms. Appl. Microbiol. Biotechnol. 60, 495-506.
Volkman, J.K. (1986) A review of sterol markers for marine and terrigenous organic matter. Organic Geochemistry 9, 83-99.
Volkman, J.K. (2005) Sterols and other triterpenoids: source specificity and evolution of biosynthetic pathways. Organic Geochemistry 36, 139-159.
Volkman, J.K., Allen, D.I., Stevenson, P.L. and Burton, H.R. (1986) Bacterial and algal hydrocarbons in sediments from a saline Antarctic lake, Ace Lake. Organic Geochemistry 10, 671-681.
Volkman, J.K., Barrett, S.M., Blackburn, S.I., Mansour, M.P., Sikes, E.L. and Gelin, F. (1998) Microalgal biomarkers: A review of recent research developments. Organic Geochemistry 29, 1163-1179.
Volkman, J.K., Barrett, S.M., Dunstan, G.A. and Jeffrey, S.W. (1993) Geochemical significance of the occurrence of dinosterol and other 4-methyl sterols in a marine diatom. Organic Geochemistry 20, 7-15.
Vuille, M., Burns, S.J., Taylor, B.L., Cruz, F.W., Bird, B.W., Abbott, M.B., Kanner, L.C., Cheng, H. and Novello, V.F. (2012) A review of the South American monsoon history as recorded in stable isotopic proxies over the past two millennia. Climate of the Past 8, 1309-1321.
Wakeham, S.G. (1989) Reduction of stenols to stanols in particulate matter at oxic–anoxic boundaries in sea water. Nature 342, 787-790.
Weiss, G.M., Pfannerstill, E.Y., Schouten, S., Sinninghe Damsté, J.S. and van der Meer, M.T.J. (2017) Effects of alkalinity and salinity at low and high light intensity on hydrogen isotope fractionation of long-chain alkenones produced by Emiliania huxleyi. Biogeosciences 14, 5693-5704.
Welander, P.V., Coleman, M.L., Sessions, A.L., Summons, R.E. and Newman, D.K. (2010) Identification of a methylase required for 2-methylhopanoid production and implications for the interpretation of sedimentary hopanes. Proceedings of the National Academy of Sciences 107, 8537-8542.
Wen-Yen, H. and Meinschein, W.G. (1976) Sterols as source indicators of organic materials in sediments. Geochimica et Cosmochimica Acta 40, 323-330.
Wester, L., Juvik, J.O. and Holthus, P. (1992) Vegetation history of Washington Island (Teraina), Northern Line Islands. Atoll Research Bulletin 358, 1 - 50.
Wolhowe, M., Prahl, F., Probert, I. and Maldonado, M. (2009) Growth phase dependent hydrogen isotopic fractionation in alkenone-producing haptophytes. Biogeosciences 6, 4165-4200.

1236 Wolhowe, M.D., Prahl, F.G., Langer, G., Oviedo, A.M. and Ziveri, P. (2015) Alkenone δD as an
1237 ecological indicator: A culture and field study of physiologically-controlled chemical and
1238 hydrogen-isotopic variation in C37 alkenones. Geochimica et Cosmochimica Acta 162, 166-182.
1239 Xu, Y. and Jaffé, R. (2008) Biomarker-based paleo-record of environmental change for an eutrophic,
1240 tropical freshwater lake, Lake Valencia, Venezuela. Journal of Paleolimnology 40, 179-194.
1241 Yan, H., Wei, W., Soon, W., An, Z., Zhou, W., Liu, Z., Wang, Y. and Carter, R.M. (2015) Dynamics of
1242 the intertropical convergence zone over the western Pacific during the Little Ice Age. Nature
1243 Geosci 8, 315-320.
1244 Yu, B. and Lin, H. (2016) Tropical Atmospheric Forcing of the Wintertime North Atlantic Oscillation.
1245 Journal of Climate 29, 1755-1772.
1246 Zhang, P., Cheng, H., Edwards, R.L., Chen, F., Wang, Y., Yang, X., Liu, J., Tan, M., Wang, X., Liu, J.,
1247 An, C., Dai, Z., Zhou, J., Zhang, D., Jia, J., Jin, L. and Johnson, K.R. (2008) A Test of Climate,
1248 Sun, and Culture Relationships from an 1810-Year Chinese Cave Record. Science 322, 940-942.
1249 Zhang, Z., Leduc, G. and Sachs, J.P. (2014) El Niño evolution during the Holocene revealed by a
1250 biomarker rain gauge in the Galápagos Islands. Earth and Planetary Science Letters 404, 420-434.
1251 Zhang, Z. and Sachs, J.P. (2007) Hydrogen isotope fractionation in freshwater algae: I. Variations among
1252 lipids and species. Organic Geochemistry 38, 582-608.
1253 Zhang, Z.H., Sachs, J.P. and Marchetti, A. (2009) Hydrogen isotope fractionation in freshwater and
1254 marine algae: II. Temperature and nitrogen limited growth rate effects. Organic Geochemistry 40,
1255 428-439.

1256

Fig. 1: Map of (A) the Northern Line Islands in the (B) central tropical North Pacific Ocean. (C) Satellite image of Washington Island showing the location of the Washington Lake sediment core WL2 and the peat bog sediment core W-BG1-PTC. Images from Google Earth.

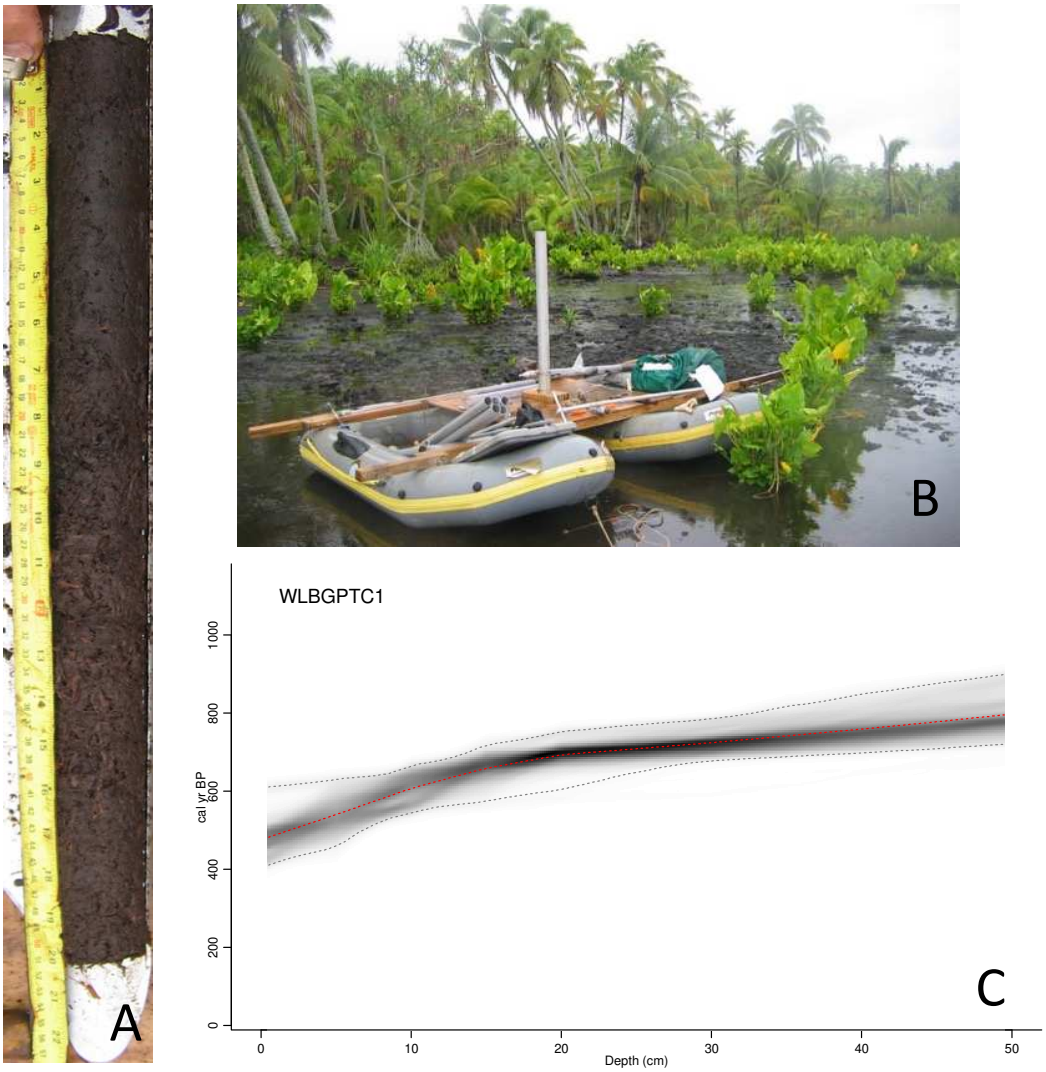

Fig. 2: (**A**) Photograph of peat core WL-BGB-PTC1 immediately after collection. (**B**) Photograph of coring site in the eastern peat bog on Washington Island. (**C**) Bayesian age model (built using Bacon 2.2, IntCal13 (Blaauw and Christen, 2011)) for Washington Island peat core WL-BGP-PTC1 based on 6 ^{14}C dates (3 on bulk OM, 3 on humin). An age of 285 yr BP (1665

CE) for the 0-1 cm sediment implies either non-deposition during the 340 years from 1665 to 2005 CE or diagenetic losses of the modern material.

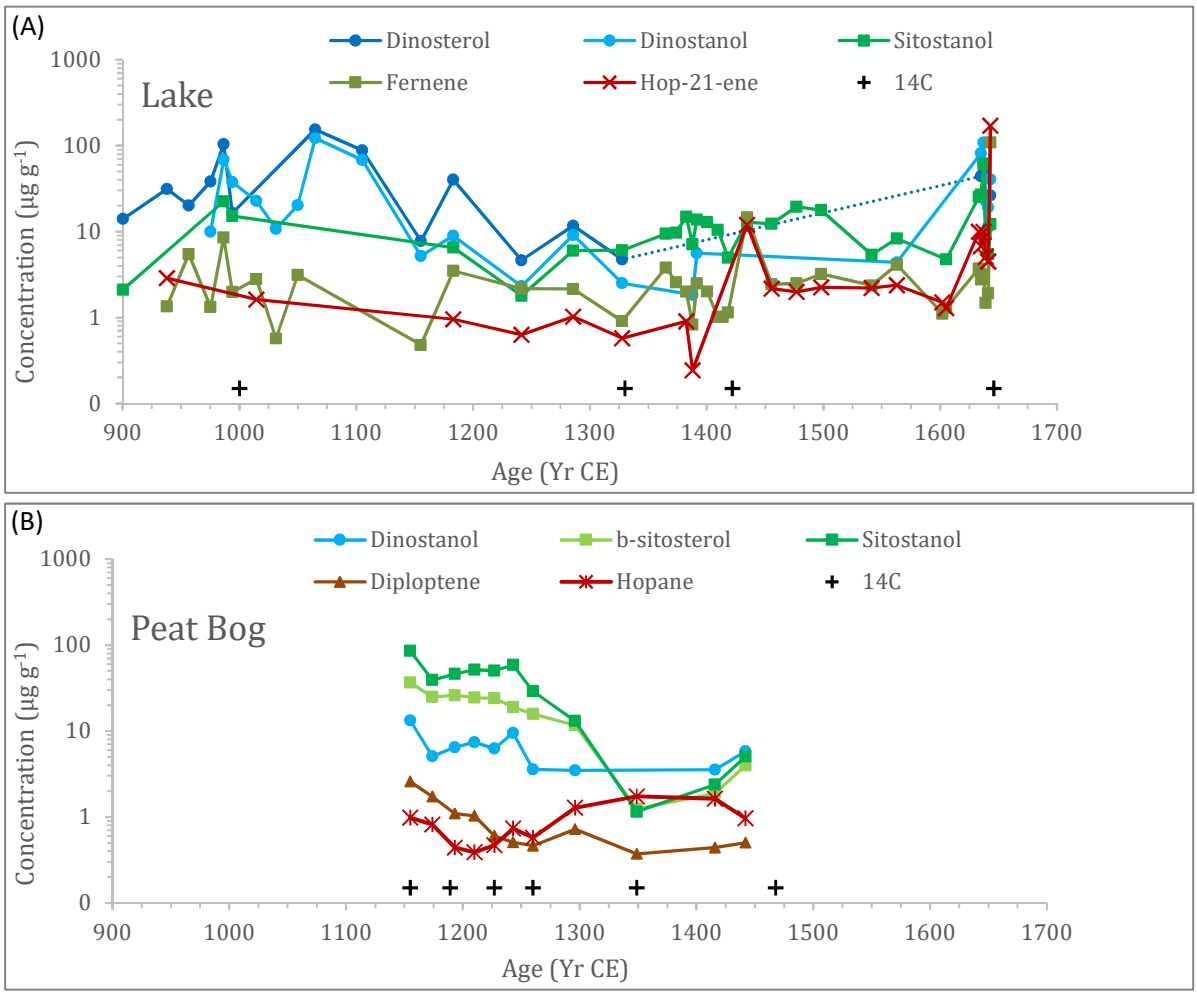

Fig. 3: Concentrations of triterpenoid lipids in Washington Island lake and peat sediments. Triterpenoid concentrations as a function of age in (**A**) Washington Lake sediment and (**B**) eastern peat bog sediment. Green symbols represent vascular plant lipids. Blue symbols represent phytoplankton lipids. Brown and red symbols represent microbial lipids. A Dotted line connects data points separated by >250 yr. Plus signs indicate depths of ^{14}C ages.

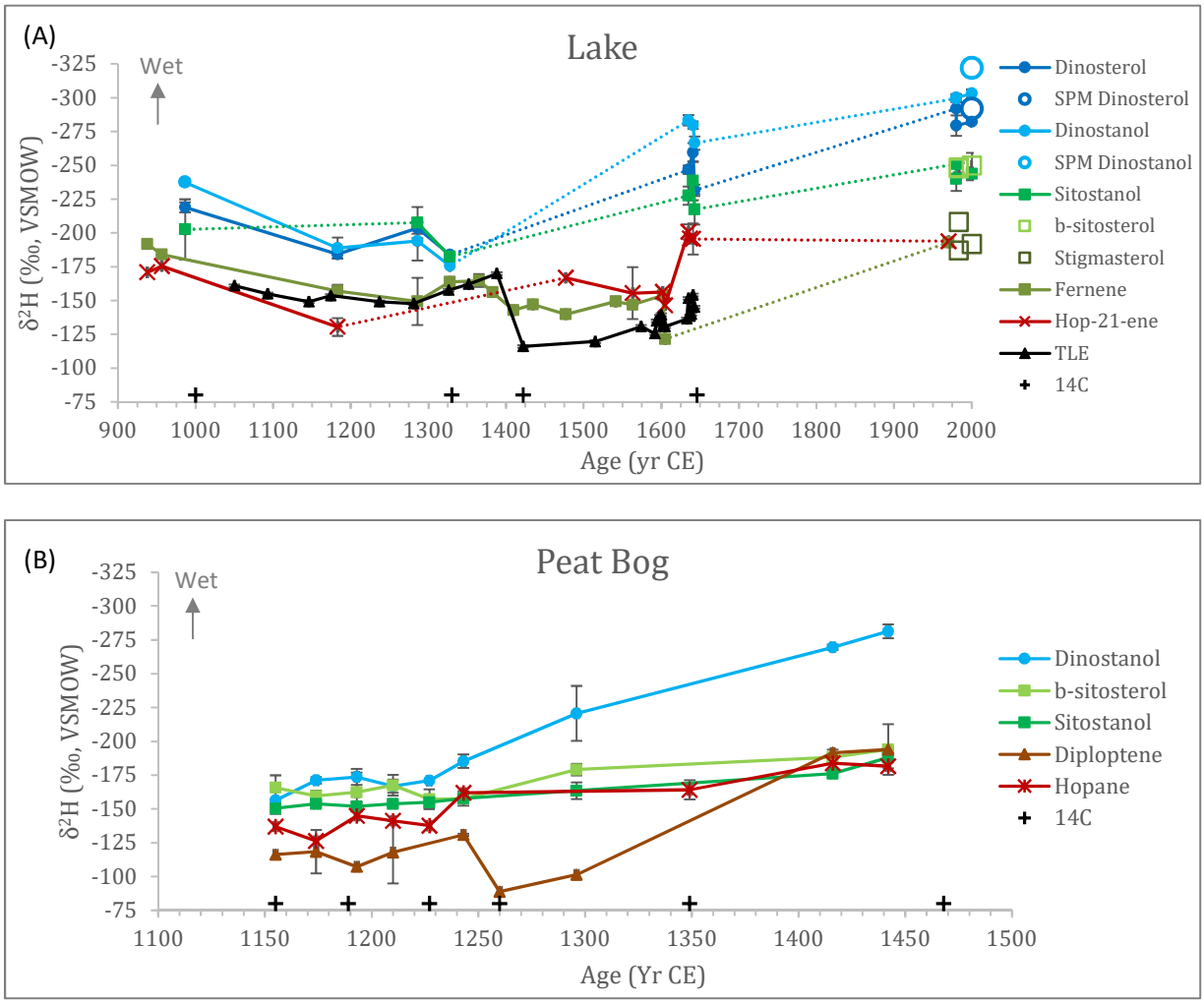

Fig. 4: Hydrogen isotopic values of triterpenoid lipids in Washington Lake and peat bog sediments. (**A**) δ^2H values of individual triterpenoids and the total lipid extract (TLE; Sachs et al., 2009) in Washington Lake sediments. δ^2H values of lipids extracted from suspended particles in lake surface waters are shown by open symbols. (**B**) δ^2H values of individual triterpenoids in the eastern peat bog sediments. Blue circles represent phytoplankton lipids (dinosterol, dinostanol). Green and gray squares represent vascular plant and algal lipids (sitostanol, β-sitosterol, stigmasterol, fernene). Red crosses represent microbial lipids. Dotted lines connect data points separated by >250 yr. Plus signs indicate depths of ^{14}C ages.

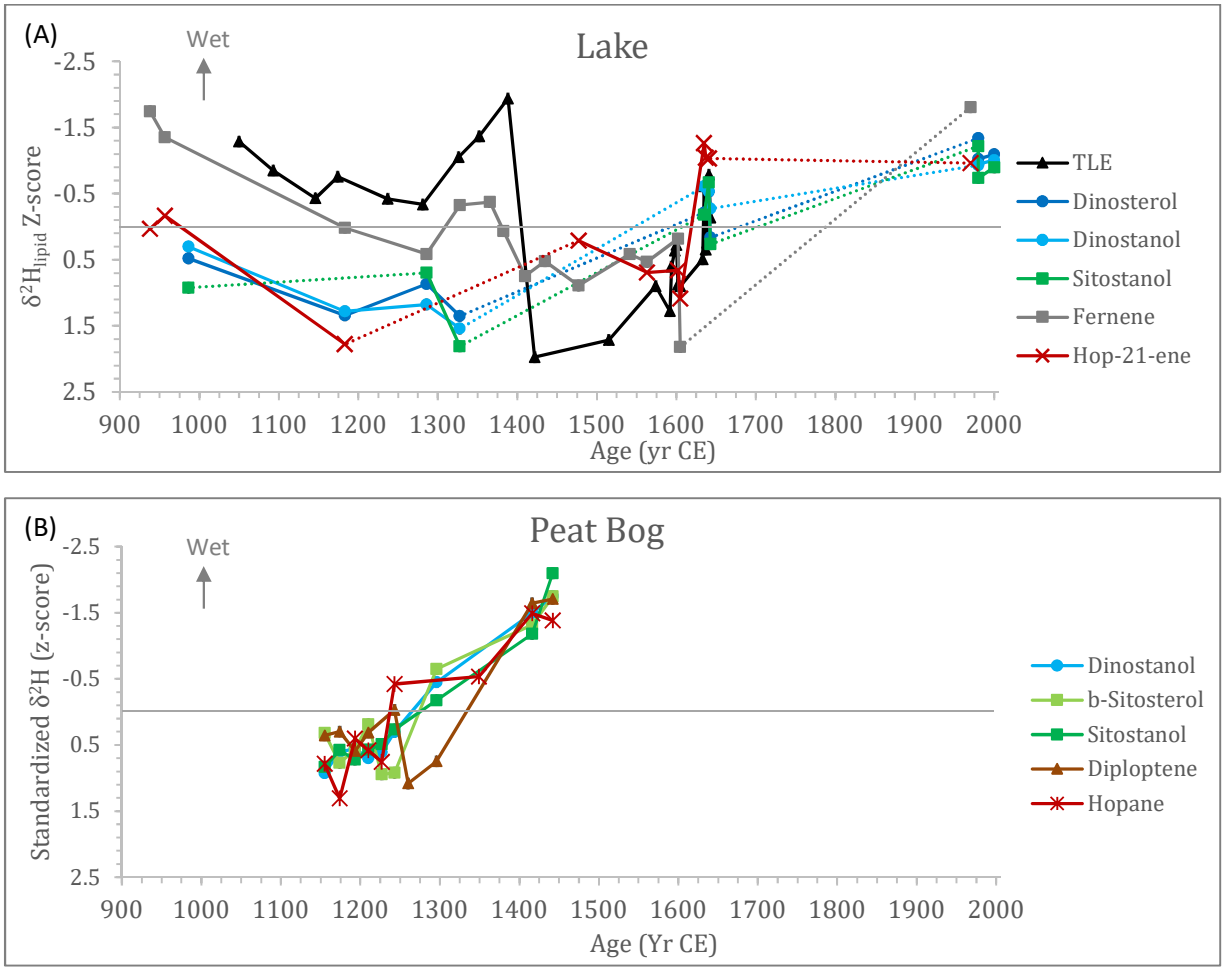

Fig. 5: Standardized hydrogen isotopic values of lipids as a function of age in Washington Lake and peat bog sediments. (**A**) Standardized hydrogen isotopic values of Washington Lake sedimentary lipids. (**B**) Standardized hydrogen isotopic values of peat core lipids. Blue circles represent phytoplankton lipids (dinosterol, dinostanol). Green and gray squares represent vascular plant and algal lipids (sitostanol, β-sitosterol, stigmasterol, fernene). Red crosses represent microbial lipids. Dotted lines connect data points separated by > 250 yr.

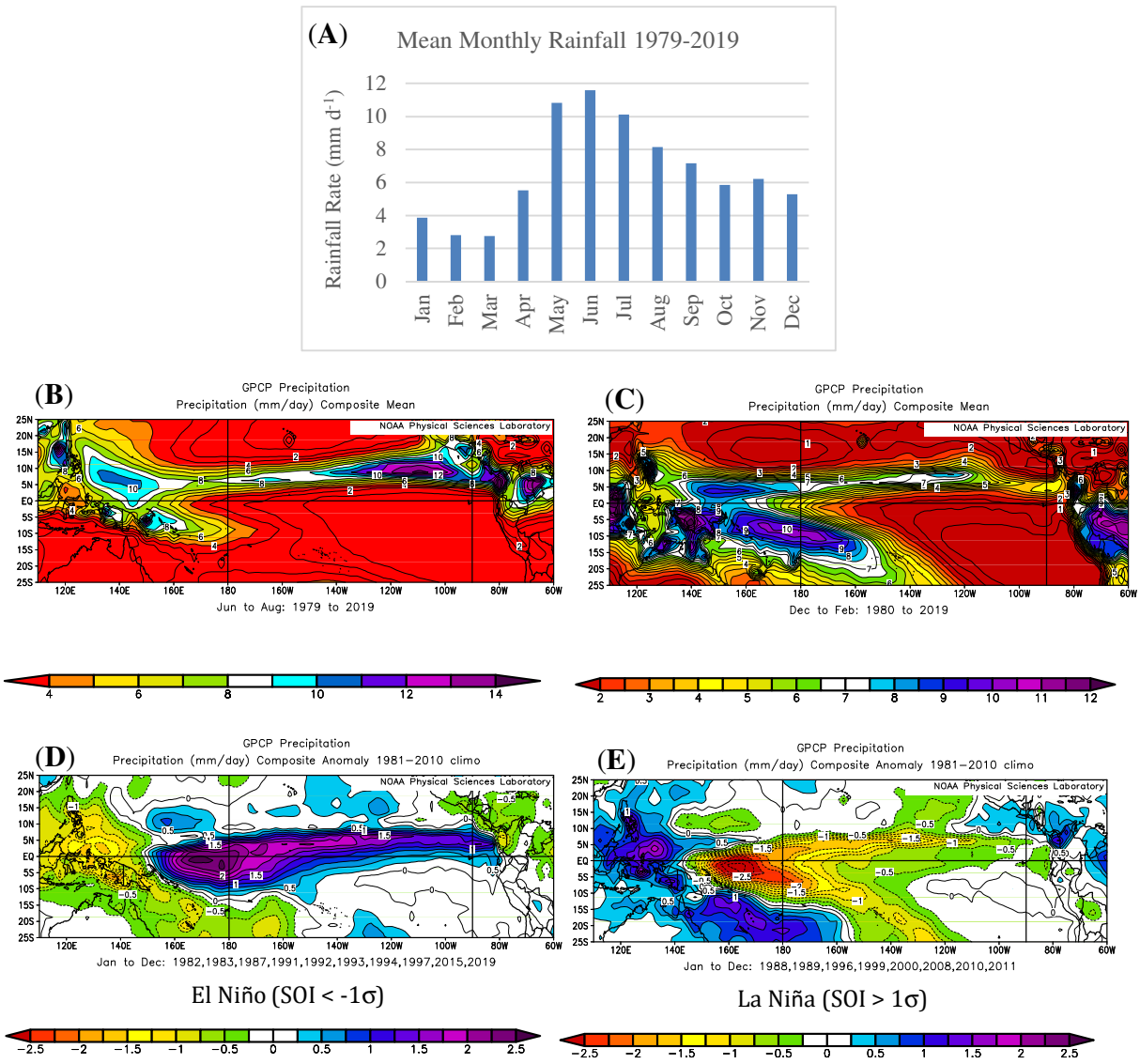

Fig. 6: Monthly, seasonal, and ENSO-related rainfall near Washington Island from the Global Precipitation Climatology Project (GPCP) v2.3 (Adler et al., 2018). (**A**) Average monthly rainfall rate in 2.5-5°N, 160-162.5°W grid cell from 1979-2019 from GPCP v2.3. Average boreal (**B**) summer (June-August) and (**C**) winter (December-February) rainfall over tropical Pacific 1979-2019. Annual rainfall anomaly associated with (**D**) El Niño (SOI < -1σ) and (**E**) La Niña (SOI > 1σ) years between 1980-2019, relative to 1981-2010 mean. Data extracted from the NOAA/ESRL Physical Sciences Laboratory, Boulder, Colorado, from their website at http://psl.noaa.gov/.

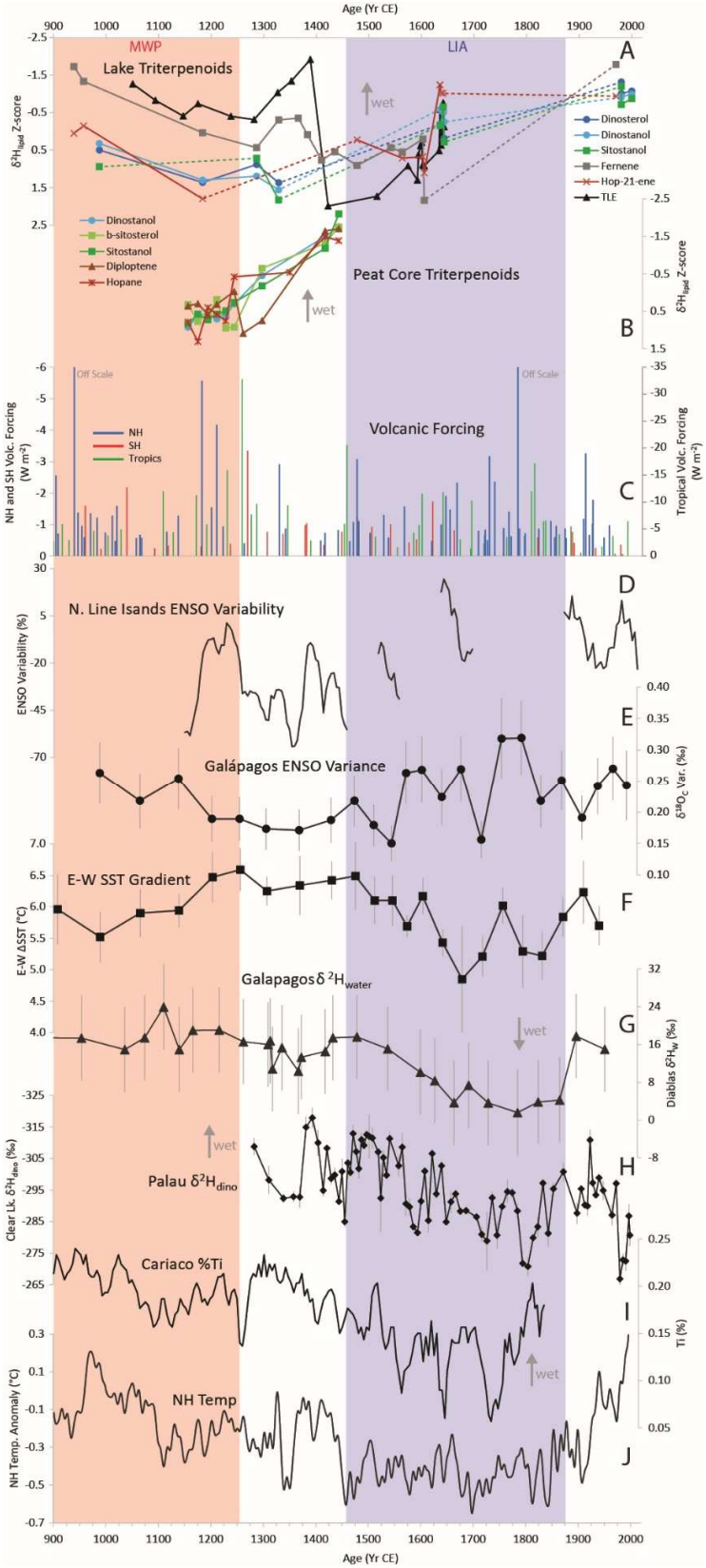
Age (Yr CE)
MWP
LIA
A
Lake Triterpenoids
wet
Dinosterol
Dinostanol
Sitostanol
Fernene
Hop-21-ene
TLE
Dinostanol
b-sitosterol
Sitostanol
Diploptene
Hopane
Peat Core Triterpenoids
wet
B
Off Scale
Off Scale
NH
SH
Tropics
Volcanic Forcing
C
D
N. Line Isands ENSO Variability
E
Galápagos ENSO Variance
E-W SST Gradient
F
Galapagos δ 2Hwater
wet
G
wet
Palau δ2Hdino
H
Cariaco %Ti
I
wet
NH Temp
J
Age (Yr CE)

Fig. 7: Regional and global climate changes during the last millennium. Standardized δ^2H values of a diverse set of triterpenoid lipids from the lake (**A**) and peat bog (**B**) on Washington Island (data gaps > 250 yr are dashed). (**C**) Radiative forcing from volcanic aerosols erupted in the Southern (red) and Northern (blue) hemispheres, and within tropical latitudes (green) from Sigl et al. (2015). (**D**) ENSO variance relative to 1961-1990 mean (moving 30-yr standard deviation expressed as a percentage change relative to the reference period, 5 yr time steps)) reconstructed from Northern Line Islands coral $\delta^{18}O$ values (Abram et al., 2020; Cobb et al., 2003; Cobb et al., 2013; Dee et al., 2020; Grothe et al., 2019). (**E**) ENSO variance reconstructed from single foraminiferal $\delta^{18}O$ values near the Galápagos by Rustic et al. (2015). (**F**) Zonal SST gradient across the equatorial Pacific reconstructed from Mg/Ca in planktonic foraminifera by Rustic et al. (2015). (**G**) Reconstructed δ^2H values of water in Diablas Lake, Galápagos, derived from the δ^2H values of algal and mangrove lipids by Nelson & Sachs (2016). (**H**) δ^2H values of dinosterol from Clear Lake, Palau from Richey & Sachs (2016). (**I**) Titanium concentration in Cariaco Basin sediments from Haug et al. (2001). (**J**) Reconstructed Northern Hemisphere temperature anomaly relative to 1961-1990 CE mean from Mann et al. (2008, 2009). Red and blue shaded regions correspond to the approximate durations of the Medieval Warm Period and Little Ice Age, respectively.

Table 1: Water δ^2H values measured in rain, lake, and seawater samples from Washington Island during 2005 sampling campaign.

Type	Name	Location	Date	δ^2H (‰)	Notes
Rain	WR1	Offshore	2005-07-08	-5.83	Departing island
Rain	WR2	Village	2005-07-06	-21.08	6:30 AM local
Rain	WR3	Lake	2005-07-06	-33.66	12:30 PM local
Rain	WR4	Lake	2005-07-06	-27.65	11:30 AM local
Lake	WL	Lake	2005-07-06	-6.72	Surface Water
Seawater	S1	2°N, 158°W	2005-07-08	2.73	Surface Water
Seawater	S2	4°N, 159°W	2005-07-10	2.73	Surface Water

Table 2: ^{14}C data for peat core WL-BG-PTC1. Bayesian age model created using Bacon 2.2 with IntCal13 radiocarbon calibration (Blaauw and Christen, 2011).

								Bacon Age Model	
Sample	**Depth (cm)**	**Material**	**Lab Code**	**fM**	**±**	**^{14}C Age**	**±**	**Age (yr BP)**	**Cal Age (yr CE)**
WL-BG-PTC1 0-1	0.5	Bulk C_{org}	CAMS-146085	0.9703	0.0037	240	35	482	1468
WL-BG-PTC1 9-10	9.5	Humin	D-AMS 037636	0.9283	0.0037	598	32	601	1349
WL-BG-PTC1 19-20	19.5	Humin	D-AMS 037637	0.8941	0.0028	899	25	690	1260
WL-BG-PTC1 29-30	29.5	Humin	D-AMS 037638	0.9054	0.0030	798	27	723	1227
WL-BG-PTC1 40-41	40.5	Bulk C_{org}	CAMS-146086	0.9199	0.0214	670	190	761	1189
WL-BG-PTC1 49-50	49.5	Bulk C_{org}	CAMS-143407	0.9164	0.0036	700	35	795	1155

Table 3: Triterpenoid occurrence in plant leaf samples from shoreline adjacent to Washington Island peat bog and lake coring sites, from near-surface sediments in each core, and from suspended particles in lake surface water. Images of plants can be found in **Fig. S1**. Occurrence based on high-probability match to published mass spectral data. Most likely biological source based on published studies as described in Sec. 3.1.

			VASCULAR PLANTS				BACTERIA			MICROALGAE	
			Plants & Algae			Ferns	Bacteria			Phytoplankton	
Smpl Type	Sample name	Plant species (Family) [type]	β-sitosterol	Stigmasterol	Sitostanol[4]	Fern-7-ene	Diplopt ene[3]	Hop-21-ene	C_{27} Hopane	Dinosterol[1]	Dinostanol[2]
Peat Plant	DSP2 (W-E)	*Scirpus littoralis* (Cyperaceae) [sedge]	✓	✓							
	DSP3 (W-D)	*Microsorum cf scolopendrium* (Polypodiaceae) [fern]	✓	✓		✓	✓	✓			
	DSP4 (W-B)	*Pandanus tectorius* (Pandanaceae) [tree]	✓	✓							
	DSP1 (W-A)	Triangular leaf plant	✓	✓							
Peat Surf Sed	0-1 cm		✓	✓	✓	✓	✓	✓	✓		✓
Lake Plant	DSP5	*Cocos nucifera*-1 (Arecaceae) [palm]	✓	✓							
	DSP7	*Cocos nucifera*-2 (Arecaceae) [palm]	✓	✓							
	DSP8	*Cocos nucifera*-3 (Arecaceae) [palm]	✓	✓							
	DSP6	*Blechnum* sp. (Blechnaceae) [fern]	✓	✓		✓	✓				
	DSP9	*Asplenium nidus* (Aspleniaceae) [fern]	✓	✓		✓	✓				
	DSP10	*Microsorum* sp. (Polypodiaceae) [fern]	✓	✓		✓	✓				
Lake Susp Partic	WL-GFF1+2		✓	✓	✓					✓	✓
Lake Surf Sed	0-5 cm		✓	✓	✓	✓	✓	✓		✓	✓

[1] 4α -23,24-trimethyl-5α-cholest-22E-en-3β-ol [2] 4α-methyl-24-ethyl-5α-cholestan-3β-ol [3] hop-22(29)-ene [4] aka Stigmastanol

Table 4: Lipid concentrations in µg (g dry weight of sediment)$^{-1}$ in Washington Island Lake sediment core WL2.

Depth (cm)	Age (yr CE)	Sitostanol (µg g^{-1})	Dinosterol (µg g^{-1})	Dinostanol (µg g^{-1})	Hop-21-ene (µg g^{-1})	Fernene (µg g^{-1})
112	1643	12.2	26.2	40.5	171	108
113	1641	5.45	11.3	19.1	4.49	1.92
114	1639	9.51	8.54	22.7	5.06	1.49
115	1637	61.6	48.1	109	9.87	3.18
116	1635	27.0	44.1	81.7	6.72	2.75
117	1633	25.3			10.0	3.69
130	1605	4.73			1.30	1.29
131	1602				1.50	1.12
132	1600					
133	1598					
135	1594					
136	1592					
145	1574					
150	1563	8.28		4.36	2.38	4.12
160	1541	5.38			2.20	2.36
172	1515					
173	1513					
180	1498	17.8			2.25	3.20
190	1477	19.5			2.00	2.50
200	1456	12.3			2.16	2.44
210	1435	12.9			12.0	14.6
216	1422					
220	1418	4.96				1.15
225	1414					1.01
230	1409	10.5				1.01
240	1401	12.8				2.01
250	1392	13.9		5.60		2.49
254	1388	7.14		1.83	0.24	0.83
260	1383	14.9			0.90	1.99
270	1374	9.75				2.57
280	1365	9.43				3.82
295	1352					
323	1328	6.06	4.74	2.53	0.58	0.91
350	1286	6.02	11.8	9.12	1.03	2.14
379	1242	1.80	4.64	2.32	0.63	2.16
418	1183	6.55	40.2	8.95	0.96	3.49
436	1155		7.77	5.19		0.48

469	1105		88.5	68.2		
492	1065		154	122		
500	1050			20.4		3.14
510	1031			10.8		0.57
519	1014			22.9	1.61	2.80
530	994	15.2	16.4	37.7		1.98
534	986	22.4	105	68.9		8.55
540	975		38.2	10.0		1.33
550	957		20.1			5.47
560	938		31.2		2.88	1.35
580	900	2.11	14.1			

Table 5: Lipid concentrations in µg (g dry weight of sediment)$^{-1}$ in Washington Island peat core WL-BG-PTC1.

Depth (cm)	Age (yr CE)	ß-Sitosterol (µg g^{-1})	Sitostanol (Stigmastanol) (µg g^{-1})	Dinostanol (µg g^{-1})	Diploptene (µg g^{-1})	C_{27} Hopane (µg g^{-1})
3	1637	3.99	5.02	5.81	0.50	0.96
5	1621	1.88	2.37	3.56	0.44	1.63
10	1580	1.24	1.15		0.37	1.73
15	1540	11.7	13.0	3.49	0.72	1.28
20	1500	15.8	29.2	3.58	0.46	0.58
25	1459	19.0	58.5	9.52	0.51	0.73
30	1419	24.0	50.6	6.25	0.60	0.47
35	1378	24.5	51.9	7.40	1.03	0.39
40	1338	26.3	45.9	6.44	1.10	0.44
45	1297	24.9	39.3	5.08	1.73	0.82
50	1257	36.7	85.2	13.3	2.57	0.98

Table 6: δ^2H values of lipids in Washington Lake core WL2.

		ß-sitosterol		**Stigmasterol**		**Sitostanol**		**Dinosterol**		**Dinostanol**		**Hop-21-ene**		**Fernene**		**TLE**[2]
Depth (cm)	Age (yr CE)[1]	δ^2H (‰)	SD	δ^2H (‰)	SD	δ^2H (‰)	SD	δ^2H (‰)	SD	δ^2H (‰)	SD	δ^2H (‰)	SD	δ^2H (‰)	SD	δ^2H (‰)
0.5	2005	-250	9.5	-192	0.3	-244	4.7	-282	2.0	-303	3.0	-194	1.5	-193	2.8	
10	1825	-248	3.5	-187	0.9	-240	8.9	-279	7.6	-300	2.6					
15	1825	-248	4.3	-208	8.2	-251	1.7	-292	0.1	-299	2.7					
112	1643					-217	11.3	-231	4.1	-266	4.8					-145
113	1641											-195	11.5			-154
114	1639															-140
115	1637					-239	14.4	-259	6.9	-280	2.8	-196	2.9			-138
116	1635					-227	6.7	-247	3.1	-283	3.9	-201	5.6			-152
117	1633															-136
130	1605											-146		-121		-131
131	1602											-156		-154		-131
132	1600															-139
133	1598															-138
135	1594															-135
136	1592															-126
145	1574															-131
150	1563											-156	19.2	-147	0.4	
160	1541												2.3	-149		
172	1515															-120
190	1477											-167		-140		
210	1435													-147		
216	1422															-116
230	1409													-143		
254	1388															-170
260	1383													-156		
280	1365													-165	4.8	
295	1352															-162
323	1328					-182		-184		-175				-164		
325	1326															-158
350	1286					-208	11.6	-203	4.1	-194	14.3			-149	17.5	
353	1281															-148
382	1237															-149
418	1183							-184	3.0	-189	7.8	-130	6.6	-157	4.6	
424	1174															-154
442	1146															-149
477	1093															-155

500	1050															-161
534	986					-203	22.3	-219	3.7	-238	2.2					
550	957											-175		-184		
560	938											-171		-192		

[1] Core top age estimated at 2005 CE, the year of collection. Average age of 0-112 cm sediment, that contains bomb ^{14}C throughout, estimated to be 1825 CE owing to extensive bioturbation. See Sec. 2.6 for further discussion.
[2] TLE δ^2H data from Sachs et al. (2009)

Table 7: δ^2H values and concentrations of phytoplankton lipids dinosterol and dinostanol in suspended particles from surface waters of Washington Lake in July 2005.

	Dinosterol			**Dinostanol**		
	Conc.	δ^2H		Conc.	δ^2H	
Sample	ng L^{-1}	‰	SD	ng L^{-1}	‰	SD
WL2-GFF1	51	-294		350	-318	3.4
WL2-GFF2	53	-290		237	-326	2.7
Mean	52	-292	2.8	294	-322	6

Table 8: δ^2H values of lipids in Washington Island peat core WL-BG-PTC1.

		ß-sitosterol		**Sitostanol**		**Dinostanol**		**Diploptene**		**C_{27} Hopane**	
Depth (cm)	Age (yr CE)	δ^2H (‰)	SD (‰)	δ^2H (‰)	SD (‰)	δ^2H (‰)	SD (‰)	δ^2H (‰)	SD (‰)	δ^2H (‰)	SD (‰)
3	1637	-194	0.1	-188	8.0	-281	5.1	-194	18.7	-182	7.1
5	1621	-188		-176		-270	2.0	-191	2.4	-184	3.2
10	1580									-164	9.5
15	1540	-179	4.3	-163	6.1	-221	20.3	-101			
20	1500							-89			
25	1459	-158	2.7	-158	5.3	-185	5.1	-131	0.8	-162	
30	1419	-157	7.3	-155	4.2	-171				-138	
35	1378	-168	7.7	-154	1.9	-167	4.9	-118	23.0	-141	
40	1338	-162	14.4	-152	2.9	-174	5.9	-107		-145	
45	1297	-160	3.8	-154	2.3	-171	2.4	-118	16.0	-126	4.8
50	1257	-166	9.1	-150	4.1	-156		-116		-137	1.6